UNIVERSITY OF ILLINOIS
LIBRARY

THE JOURNAL OF THE
ASTRONAUTICAL
SCIENCES

VOLUME VII, NO. 3 FALL 1960

CONTENTS

Charge Neutralization in an Ionic Rocket
G. G. Cloutier and T. W. Johnston 49

Ephemeris Time *T. P. Gabbard* 58

Biological Shielding for Radiation Belt Particles
D. L. Dye and J. C. Noyes 64

The Influence of Heart Action and the Circulation of Blood on Mannel Satellite Attitude Control
Lawrence R. Zeitlin 70

PUBLISHED BY THE AMERICAN ASTRONAUTICAL SOCIETY, INC.

THE AMERICAN ASTRONAUTICAL SOCIETY, INC.

516 Fifth Avenue, New York 36, New York, U.S.A.

1960 BOARD OF DIRECTORS OF SOCIETY

GEORGE R. ARTHUR, *President*
General Electric Company
WILLIAM WHITSON, *Vice President*
Daystrom, Inc.
ROBERT YOUNG, *Vice President*
Avion, Div. ACF
JOHN J. CAMPBELL, *Treasurer*
Radio Corp. of America
FERNAND F. MARTIN, *Secretary*
Radio Corp. of America
COL. PAUL BUTMAN, (1960)
USAF—ARDC
JOHN CRONE, (1960)
Airtronics, Inc.
MAJ. GEN. WILLIAM W. DICK, JR., (1960)
USA—Office of Army Research
EDWARD H. HEINEMANN, (1960)
Douglas Aircraft Co.
ROBERT E. ROBERSON, (1960)
Systems Corp. of America
CMDR. MALCOLM D. ROSS, (1960)
USN—Office of Naval Research
SYDNEY S. SHERBY, (1960)
Hiller Aircraft Corporation
ROSS FLEISIG, (1961)
Sperry Gyroscope Co.
ROBERT P. HAVILAND, (1961)
General Electric Co.
ALEXANDER KARTVELI, (1961)
Republic Aviation Corp.
DONALD H. MENZEL, (1961)
Harvard University
AUSTIN N. STANTON, (1961)
Varo Manufacturing Co.
ERNST STUHLINGER, (1961)
Army Ballistic Missile Agency
ROBERT M. BRIDGFORTH, JR., (1962)
Boeing Airplane Co.
COL. PAUL A. CAMPBELL, (1962)
USAF—School of Aviation Medicine
BRIG. GEN. ROBERT E. GREER, (1962)
United States Air Force
ALFRED M. MAYO, (1962)
Douglas Aircraft Co.
NORMAN V. PETERSEN, (1962)
Northrop Corp.
S. FRED SINGER, (1962)
University of Maryland
JAMES A. VAN ALLEN, (1962)
State University of Iowa

EDITORIAL ADVISORY BOARD

DR. G. GAMOW
University of Colorado
DR. F. A. HITCHCOCK,
Ohio State University
DR. A. MIELE
Boeing Scientific Research Lab.
DR. W. B. KLEMPERER,
Douglas Aircraft Co.
DR. J. M. J. KOOY,
Lector, K.M.A.
DR. I. M. LEVITT,
Franklin Institute
CDR. G. W. HOOVER,
Benson-Lehner
DR. H. O. STRUGHOLD,
USAF School of Aviation Medicine
DR. PAUL A. LIBBY,
Polytechnic Institute of Brooklyn

THE AMERICAN ASTRONAUTICAL SOCIETY

The American Astronautical Society, founded in 1953 and incorporated in New York State in 1954, is a national scientific organization dedicated to advancement of the astronautical sciences. The society considers manned interplanetary space flight a logical progression from today's high-performance research aircraft, guided missile, and earth satellite operations. The scope of the society is illustrated by a partial list of the astronautical fields of interest: astronavigation, biochemistry, celestial mechanics, cosmology, geophysics, space medicine, and upper atmosphere physics, as well as the disciplines of astronautical engineering including space vehicle design, communications, control, instrumentation, guidance, and propulsion. The aims of the society are to encourage scientific research in all fields related to astronautics and to propagate knowledge of current advances. Promotion of astronautics in this way is accomplished by the society largely through its program of technical meetings and publications.

AFFILIATIONS

AAS cooperates with other national and international scientific and engineering organizations. AAS is an affiliate of the American Association for the Advancement of Science and a member organization of the International Astronautical Federation.

MEMBERSHIP REQUIREMENTS

All persons having a sincere interest in astronautics or engaged in the practice of any branch of science, which contributes to or advances the astronautical sciences, are eligible for one of the various grades of membership in the Society. Requirements are tabulated below. A special category of Student Membership has been authorized for full time students or those under 18 years of age. A nominal membership fee of $5.00 is made in such cases to cover publications. The Directors of the Society may elect as Fellows of the Society those who have made direct and significant contributions to the astronautical sciences. Information regarding individual membership as well as Corporate and Benefactor Membership may be obtained by writing the Corresponding Secretary at the Society address.

Grade	Contribution To Astronautics	Experience or Scientific Training*	Annual Dues
Affiliate Member	Interest	none required	$8
Member	Active Interest	8 years	$10
Senior Member	Recognized Standing and Direct Contribution	10 years	$15

* A Bachelor's, Master's or Doctor's degree in any branch of science or engineering is equivalent to four, six or eight years of experience, respectively.

Journal of the Astronautical Sciences

Director of Publications, John J. Raffone
Editor, Robert E. Roberson
Managing Editor, George Clark
Associate Editor, Robert M. L. Baker, Jr.

Published quarterly by the AMERICAN ASTRONAUTICAL SOCIETY, INC. at 428 E. Preston Street, Baltimore 2, Maryland

Address all Journal correspondence to Box 24721, Los Angeles 24, Calif.

Subscription Rates: One year $5.00; foreign $6.00; single copy $1.25. The Journal is published quarterly. Members of the Society receive the Journal as a part of their dues.

Application to mail at second class postage rates is pending at Baltimore, Maryland.

Copyright 1960, by THE AMERICAN ASTRONAUTICAL SOCIETY, INC.

Charge Neutralization in an Ionic Rocket

G. G. Cloutier and T. W. Johnston*

bstract

An ionic rocket model is considered in which ions are ected from an ideal plane diode. Charge neutralization of e ion beam is accomplished by means of electrons injected ound the ion beam. The potential within the ion beam in the esence of electrons is studied as an electrostatic problem. xial and radial solutions are given for various charge distri-itions. It is found that the potential at the centre of the beam pends primarily on the charge per unit length unless com-ete neutralization is accomplished very rapidly.

The power and thrust of an ionic rocket is studied in terms the parameters of an ideal plane diode. Considerations of e potential depression within the diode indicate that the wer and thrust deteriorate very rapidly for diode spacings ss than one-half the radius of the beam. For these same diode acings, the reduction in the ion diode efficiency due to the ectrostatic force of the partially neutralized beam becomes ry important.

Considerations are given for the optimum choice of diode rameters. A numerical example illustrates the relative im-rtance of the various factors. The process of charge mixing discussed in view of the approximations made.

ntroduction

It is well known that the useful part of the exhaust an ionic (i.e. ion diode) rocket must contain equal nounts of positive and negative charge and that any cess will be electrostatically attracted back to the cket and thus contribute no thrust. If a planar diode infinite cross section is considered as the diode celerator, it seems that intimate charge mixing should ke place within a distance which is small compared th the electrode spacing. For practical current nsities and voltages this spacing will be very small d mixing within this distance very difficult if not possible.

This limitation is however only severe in an infinite de. In a diode of finite area the allowable distance charge separation is increased as the ratio of diode ea to square of the spacing is decreased. The actual ometry of the ion and neutralizing electron beams n also be more readily treated in a model with a ite area.

It will be seen that the space charge effects in the de are of the same order as the exhaust charge-paration effects for an electron beam with area of the me order as the ion beam area; both are reduced by lucing the area for a given spacing. The ideal thrust, glecting charge effects, for a given diode spacing and voltage varies directly as the diode area, but reductions from the ideal thrust due to space charge effects are also more noticeable as the area is increased. In other words, a very large area diode with severe charge limitations can, with advantage, be subdivided into smaller diodes until the point of diminishing returns is reached, where further subdivision produces negligible improvement in thrust for the added complexity of the structure.

The charge-separation effect in the exhaust will be examined by considering an ionic rocket in which ions are ejected from an ideal plane diode of circular cross-section. It will be assumed that the charge neutralization is accomplished by means of electrons injected around the ion beam. Because of the electric field across the ion beam the electrons will oscillate radially through the beam with the result that they will form a cylinder of negative charge concentric with the ion beam. The potential within the ion beam in the presence of electrons will be treated as the electrostatic problem of two concentric cylinders of opposite charge.

The power and thrust of an ionic rocket will then be studied in terms of a parameter (electrode spacing/beam radius) of an ideal plane diode. Now both the potential depression (charge effects) within the ionic diode and the ejection-plane image force due to incomplete charge mixing outside the diode in the exhaust will be considered.

This analysis leads to the conclusion that the electrode spacing should be in the range of 0.5 to 1 times the beam radius. It is also deduced that complete charge mixing and/or recombination further than a distance of about ten beam radii has little effect on the system. From a typical example it is found that complete neutralization will be negligible within such a distance.

Since electrical and mechanical quantities are involved in several expressions, it was found convenient to use the M.K.S. system throughout the paper.

I. Electrostatic Solutions

1. Axial solution for two concentric cylinders of opposite charge in front of an infinite conducting plane

The model to be studied is represented by two concentric cylinders of opposite charge placed in front of an infinite conducting plane. To obtain the solution for the potential along the axis of the cylinders the conducting plane is replaced by two concentric

* RCA Victor Company, Ltd., Research Laboratories, ntreal, Canada.

image cylinders as shown in Fig. 1. Since the potential is a scalar quantity, the final solution may be obtained by proper summation of the potential due to each cylinder.

a) *Uniform charge distribution*

Single cylinder. The potential at a point x_0 on the axis of a finite cylinder of positive charge is:

$$V_{x_0} = \frac{1}{4\pi\epsilon_0}\int_0^l\int_0^{r_0} \frac{q_v 2\pi r\, dr\, dx}{[(x - x_0)^2 + r^2]^{\frac{1}{2}}} \qquad (1)$$

where q_v is the volume charge density
r_0 is the radius of the cylinder
l is the length of the cylinder
ϵ_0 is the permittivity of free space.

After integration, if one defines

$q_\Lambda = q_v \pi r_0^2$, the charge per unit length
$\Lambda = l/r_0$ and $X = x_0/r_0$

the expression for the potential along the axis becomes:†

† A detailed derivation of this solution has been shown in the Research Report No. 7-811-1, Aug. 1959, RCA Victor Co. Ltd., Montreal, Canada.

$$V_{x_1} = \frac{q_\Lambda}{4\pi\epsilon_0}[(\Lambda - X)\sqrt{(\Lambda - X)^2 + 1} + X\sqrt{X^2 + 1} - (\Lambda - X)\,|\Lambda - X| - X\,|X| + \sinh^{-1}(\Lambda - X) + \sinh^{-1}(X)] \qquad (2)$$

Ion and electron cylinders and their images. The axial solution for the potential of two concentric cylinders of opposite charge in front of an infinite conducting plane is obtained by superposition of four equations of the type of Eqn. (2).

$$V_x = V_{x_1} + V_{x_2} + V_{x_3} + V_{x_4} \qquad (3)$$

where V_x is the total solution (See footnote†)
V_{x_1} is the solution for the cylinder of positive charge (r_2)
V_{x_2} is the solution for the cylinder of negative charge (r_1)
V_{x_3} is the solution for the image cylinder of negative charge (r_2)
V_{x_4} is the solution for the image cylinder of positive charge (r_1)

$$V_{x_1} = \frac{q_\Lambda}{4\pi\epsilon_0}\Big[(\Lambda - X)[(\Lambda - X)^2 + 1]^{\frac{1}{2}} X[X^2 + 1]^{\frac{1}{2}} - (\Lambda - X)\,|\Lambda - X| - X\,|X| + \sinh^{-1}(\Lambda - X) + \sinh^{-1}(X)\Big] \qquad (3a)$$

$$V_{x_2} = \frac{-q_\Lambda}{4\pi\epsilon_0}\Big[R_0(\Lambda - X)[R_0^2(\Lambda - X) + 1]^{\frac{1}{2}} + R_0 X[R_0^2 X^2 + 1]^{\frac{1}{2}} - R_0^2(\Lambda - X)\,|\Lambda - X| - R_0^2 X\,|X| + \sinh^{-1} R_0(\Lambda - X) + \sinh^{-1}(R_0 X)\Big] \qquad (3b)$$

$$V_{x_3} = \frac{-q_\Lambda}{4\pi\epsilon_0}\Big[-X[X^2 + 1]^{\frac{1}{2}} + (\Lambda + X)[(\Lambda + X)^2 + 1]^{\frac{1}{2}} + X\,|X| - (\Lambda + X)\,|\Lambda + X| - \sinh^{-1}(X) + \sinh^{-1}(\Lambda + X)\Big] \qquad (3c)$$

$$V_{x_4} = \frac{q_\Lambda}{4\pi\epsilon_0}\Big[-R_0 X[R_0^2 X^2 + 1]^{\frac{1}{2}} + R(\Lambda + X)[R_0^2(\Lambda + X)^2 + 1]^{\frac{1}{2}} + R_0^2 X\,|X| - R_0^2(\Lambda + X)\,|\Lambda + X| - \sinh^{-1}(R_0 X) + \sinh^{-1} R_0(\Lambda + X)\Big] \qquad (3d)$$

In these expressions, the length (Λ) of the cylinder and the distance (X) along the axis have been normalized to the radius (r_2) of the cylinder of positive charge. The ratio of the radii of the two concentric cylinders is expressed as $R_0 = r_1/r_2$.

The solution has been evaluated for $\Lambda = l/r_2 =$ 0.3, 3 and 30 and for $R_0 = 1.5$ and is shown on a log-log scale in Fig. 1. It is noted that for $\Lambda = 30$ (long cylinder) the conducting plane has little effect on the potential throughout the cylinders. The potential attains the same value as if the cylinders were infinitely long. However the situation is quite different if the cylinders are short ($\Lambda = 0.3$) that is when complete neutralization of the ion beam is rapidly accomplished.

b) *Linearly decreasing charge density along the axis*

To allow for gradual mixing of the charges the problem of concentric cylinders of charges has been

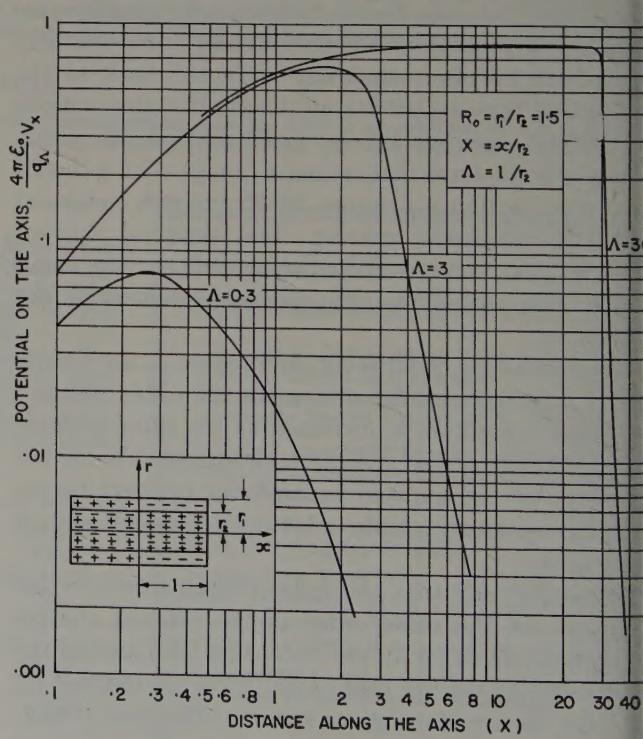


FIG. 1. Potential variation along the axis of two concentric cylinders of opposite charge in front of an infinite conducting plane.

udied for the case where the charge density is uniform ver the cross section but linearly decreasing along the xis. The solution is obtained as above (Eqn. 3) by the ethod of images. (See Footnote†.)

A plot of the potential variation along the axis for ne case $\Lambda = 30$ and $R_0 = r_1/r_2 = 1.5$ is shown in Fig. in comparison with the equivalent solution for the ase of uniform charge density throughout the cylinders. lthough the potential drops more rapidly when the harge density decreases linearly it is seen that, for = 30, the maximum value of the potential reaches 7% of that for an infinitely long cylinder. Therefore, the neutralization occurs in a distance greater than) times the radius of the beam, the theory for uniform harge distribution along the axis is adequate. As will e shown later, practical recombination or mixing istances will give values for Λ much greater than 30, curves for $\Lambda = 0.3$ and 3 were not calculated.

Radial solution for two infinitely long concentric cylinders of charge

Let us consider two concentric infinite cylinders of pposite charge. The small cylinder contains positive harges uniformly distributed throughout the volume. n the large cylinder, the negative charge density is ssumed to increase radially as the square of the radius. he solution for the potential across the two cylinders expressed in terms of two parameters: the relative adii of the cylinders (R_0) and the ratio (γ) of the egative charge densities at the centre and the edge the large cylinder. Let the charge densities be ee Fig. 3):

$$q_{v_1} = -q_{v_0}(1 + ar^2) \tag{4}$$

and

$$q_{v_2} = \frac{q_\Lambda}{r_2^2}$$

where q_{v_0} is the negative charge density at $r = 0$ and a is a parameter defined in terms of the ratio (γ) of the negative charge density at the centre and the edge of the cylinder.

$$\gamma = q_{v_0}/q_{v_{r_1}} \tag{5}$$

Equation (4) becomes:

$$q_{v_1} = -q_{v_0}\left[1 + \left(\frac{1}{\gamma} - 1\right)\left(\frac{r}{r_1}\right)^2\right]$$

q_{v_0} is defined by assuming the same charge per unit length for both cylinders:

$$q_\Lambda = -2\pi \int_0^{r_1} q_{v_1}(r) r\, dr$$

which gives upon integration:

$$q_{v_0} = \frac{q_\Lambda}{\pi r_1^2} \frac{1}{[1 + 1/2(1/\gamma - 1)]} \tag{6}$$

The electric field across the two concentric cylinders is obtained by applying Gauss's theorem. The potential is then derived by integration of the electric field along the radius of the cylinders. The constants arising from the integration are determined with the help of the following boundary conditions:

$$\text{at} \quad r = r_1, \qquad V(r_1) = 0$$
$$\text{at} \quad r = r_2, \qquad V(r_1) = V(r_2)$$

Defining $R = r/r_2$ and $R_0 = r_1/r_2$ (i.e. normalized as before to the ion beam radius) one obtains the following expressions for the potential across the cylinders.

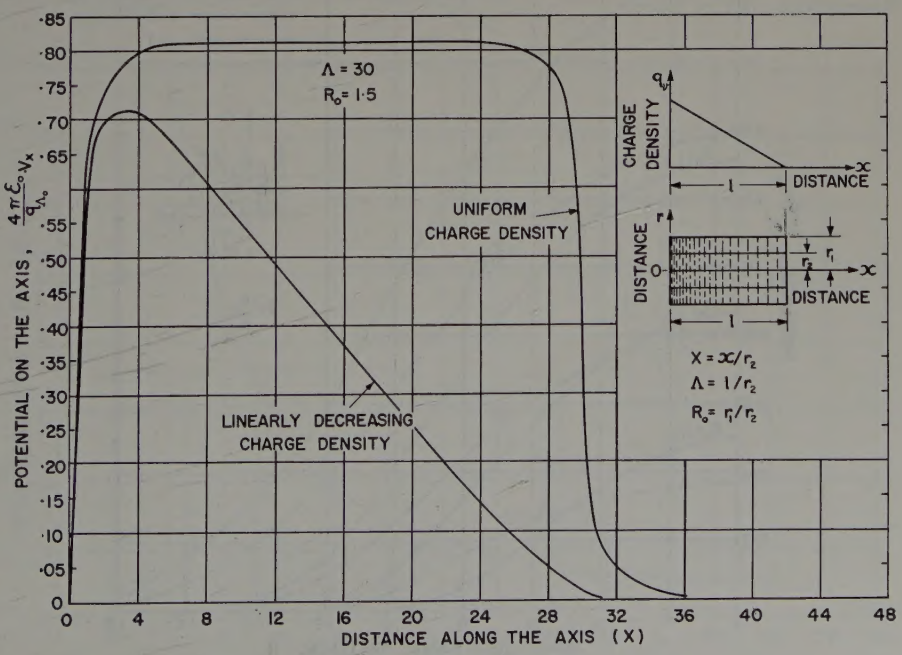


FIG. 2. Potential variation on the axis of two concentric cylinders of opposite charge in front of an infinite conducting plane. iform and linearly decreasing charge densities.

For $0 < R < 1$

$$V(R) = \frac{q_\Lambda}{4\pi\epsilon_0}\left[2 \ln R_0 + (1 - R^2) - \frac{(1 - R^2/R_0^2)}{[1 + \tfrac{1}{2}(1/\gamma - 1)]} - \frac{(1/\gamma - 1)(1 - R^4/R_0^4)}{4[1 + \tfrac{1}{2}(1/\gamma - 1)]}\right] \quad (7a)$$

For $1 < R < R_0$

$$V(R) = \frac{q_\Lambda}{4\pi\epsilon_0}\left[2 \ln (R_0/R) - \frac{(1 - R^2/R_0^2)}{[1 + \tfrac{1}{2}(1/\gamma - 1)]} - \frac{(1/\gamma - 1)(1 - R^4/R_0^4)}{4[1 + \tfrac{1}{2}(1/\gamma - 1)]}\right] \quad (7b)$$

The variation of potential across the two cylinders has been plotted for two limiting cases $\gamma = 0$ and $\gamma = 1$ (Fig. 3). The case $\gamma = 0$ represents the conditions for which most of the electrons are concentrated near the outer radius, while for $\gamma = 1$ the electrons are assumed to be distributed uniformly across the cylinder.

The mean value of the potential over the cross section of the positive cylinder may be calculated by means of the following relation:

$$\bar{V} = \frac{1}{\pi}\int_0^1 V(R) 2\pi R \, dR \quad (8)$$

For $R_0 = 1.5$, with $\gamma = 0$, $\bar{V}$ is 0.644 V_0 and with $\gamma = 1$, $\bar{V}$ is 0.657 V_0 where V_0 is the potential on the axis.

II. Power and Thrust of the Ionic Rocket

Consideration will be given to the effective powe and thrust of an ionic rocket first in terms of the po tential depression due to the space charge in the diod and then in terms of the image force due to incomplet charge neutralization of the ion beam.

1. Potential depression in an ideal plane diode

Due to the space charge in the ionic diode a radia as well as an axial potential depression exists in th beam. The axial depression limits the actual curren drawn by the diode (space charge limited flow). Th radial potential depression reduces the energy of th ions in the centre of the beam.

In order to estimate the effective power and thrus of the diode in terms of the potential depression, us will be made of the theory given by Smith and Hart man (1) and Pierce (2) for the case of an homogeneou beam of circular cross section. In the derivation of th theory the current density is assumed to be uniform across the beam while the charge density and the voltag vary. In fact, the current at the centre of the beam i smaller than that at the edge. However, since th reduction in the current at the centre of the beam wil induce a reduction of the potential depression acros the beam, it is believed that the above assumption i not unreasonable for the calculations of the effectiv power and thrust. Reduced emission at the centre o the emitting plane and reduced voltage in the aperture (lens effect) will not be considered here.

Using Pierce's notation, a potential ratio is define

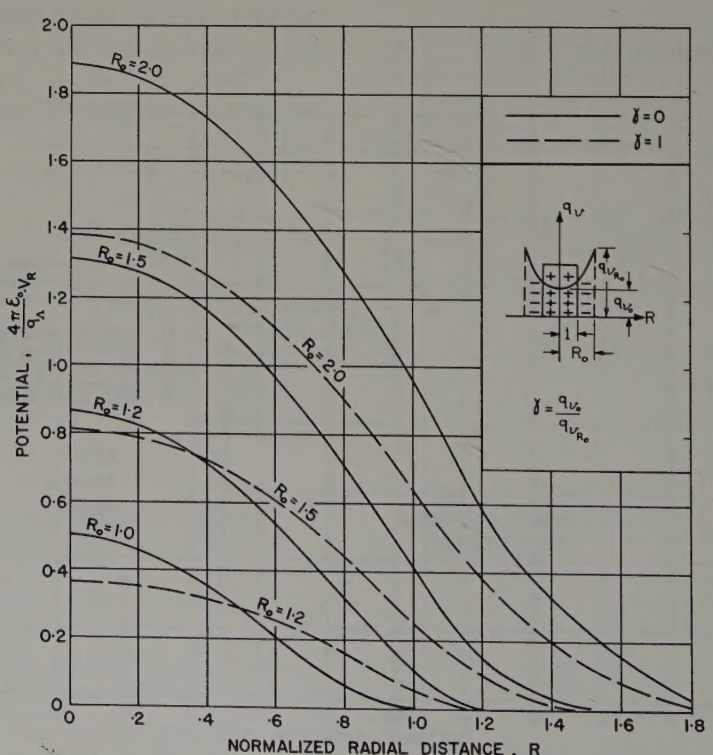


FIG. 3. Potential across two concentric infinite cylinders of opposite charge. Maximum depression of the negative charge density ($\gamma = 0$). Uniform negative charge density ($\gamma = 1$).

the ratio of the voltage at the beam edge to the ltage in the centre of the beam:

$$\phi = V/V_1$$

here V_1 is the voltage at the centre of the beam
V is the edge voltage

erce (2) has plotted ϕ as a function of a reduced dius ρ defined in the following way:

$$\rho^2 = \frac{1}{\pi\epsilon_0[2q/M]^{\frac{1}{2}}}\left(\frac{r}{a}\right)^2\left(\frac{1}{V}\right)^{3/2} \qquad (9)$$

here r is the beam radius.
a is the radius of the conducting cylinder containing the beam
In the present case "a" is the radius of the exist aperture, so $V = V_0$ the electrode voltage.
ϵ_0 is the permittivity of free space
I is the total current
q/M is the charge to mass ratio of the ions; for singly charged ions, q is the electronic charge.

et $M = 1836\ mA$, where m is the mass of the electron nd A is the atomic weight/number electron charge nd $r = a$, i.e. the beam extends over the whole aperture. For the situation of interest in the present problem here the potential ratio ϕ is close to unity, it is ssumed that $V_1 \cong V_0$ and the ion perveance can be ritten as:

$$P_i = I/V_0^{3/2} \approx I/V_1^{3/2} \qquad (10)$$

$_i$ may be expressed in terms of the electron perveance of the same diode with electron flow a function of the ructure only,

$$P_i = \frac{1}{42.8A^{\frac{1}{2}}}P \qquad (11)$$

so that the dependence of P_i on the ion mass is shown explicitly. For a plane diode of circular cross section, the electron perveance is:

$$P = \frac{7.35 \times 10^{-6}}{D^2} \qquad (12)$$

where $D = d/r$
d is the diode spacing
r is the radius of the exit aperture (ion beam radius).

Again d is normalized to the ion beam radius. Using the relations (10), (11) and (12), equation (9) becomes

$$\rho^2 = \frac{7.35 \times 10^{-6}}{(2e/m)^{\frac{1}{2}}} \cdot \frac{1}{D^2} = \frac{.445}{D^2} \qquad (13)$$

It is more convenient to define the potential depression as the ratio of the potential difference between the edge and the centre of the beam to the potential at the edge:

$$\text{Potential depression} = \frac{V_0 - V_1}{V_0} = 1 - \frac{V_1}{V_0} = 1 - \phi^{-1}$$

The potential depression ($1\text{-}\phi^{-1}$) has been plotted (Fig. 4) as function of the normalized diode spacing (D) making use of Eqn. (13) and the curve of ϕ vs. ρ given by Pierce (2).

Effective Power Ratio. The effective power of the diode can be defined as:

$$W_d = IV_e = \frac{PV_e^{5/2}}{42.8A^{\frac{1}{2}}}$$

where I is the total current
V_e is the potential of the beam averaged over the area of the exit aperture. (Strictly speaking V_e should be the square of the average of $V^{1/2}$ over the aperture, but since V_1 is close to V_0 for all useful cases, the error in this average V is small.)

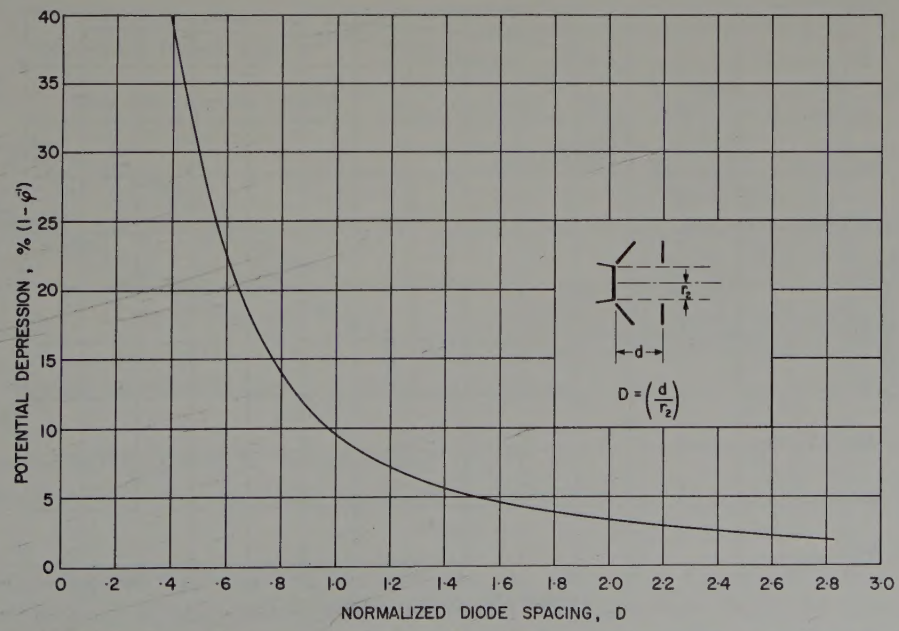


FIG. 4. Potential depression in the exit aperture of the diode as function of the normalized diode spacing

The effective power ratio is defined as the ratio of the power taking into account the potential depression across the beam to the power if the potential were uniform across the beam.

Effective power ratio

$$\text{due to diode effects} = \eta_{Wd} = \frac{W_d}{W_0} = \frac{V_e}{V_0} \quad (15)$$

Let the average of the potential depression over the cross-section be a fraction (α) of the maximum depression. Then:

$$V_e = V_0 - \alpha(1 - \phi^{-1})V_0 \quad (16)$$

and

$$\eta_{Wd} = \frac{V_e}{V_0} = 1 - \alpha(1 - \phi^{-1}) \quad (17)$$

The percentage effective power ratio has been plotted in Fig. 5 as function of the diode parameter D using Eqn. (7) and the curve $(1 - \phi^{-1})$ vs. D of Fig. 4. For this curve α was chosen as 0.657 (see Eqn. 8).

Effective Thrust Ratio. The effective thrust of the diode can be written as:

$$F_d = \frac{\dot{M}C_e}{g}$$

where the thrust is expressed in Kilograms
C_e is the ion exhaust velocity averaged over the beam
$\dot{M}$ is the mass flow rate
g is the acceleration due to gravity
In terms of current and voltage,

$$F_d = \frac{1}{g}\left(\frac{2M}{q}\right)^{\frac{1}{2}} IV_e^{\frac{1}{2}} = \frac{1}{g}\frac{PV_e^2}{47.8A^{\frac{1}{2}}} \quad (18)$$

Is the effective thrust ratio (η_{Fd}) due to diode effects if defined as the ratio of the thrust taking into account the potential depression in the beam to the thrus assuming uniform potential across the beam, ther

$$\eta_{Fd} = \frac{F_d}{F_0} = \left(\frac{V_e}{V_0}\right)^{\frac{1}{2}} \quad (19$$

Defining V_e as in Eqn. (16), η_F becomes:

$$\eta_{Fd} = [1 - \alpha(1 - \phi^{-1})]^{1/2} \quad (20$$

A curve giving the percentage effective thrust ratio a function of the normalized diode spacing is shown i Fig. 5.

Actual Thrust and Power. The ideal thrust of diode with uniform potential across the beam can b expressed as:

$$F_0 = \frac{1}{g}\left(\frac{2m}{e}\right)^{\frac{1}{2}} \times 42.8A^{\frac{1}{2}}IV_0^{\frac{1}{2}} \quad (21$$

and in terms of the electron perveance for a plane diod (using Eqns. 11 and 12)

$$F_0 = 7.35 \times 10^{-6}\frac{1}{g}\left(\frac{2m}{e}\right)^{\frac{1}{2}}\frac{V_0^2}{D_2} = 2.52 \times 10^{-12}\frac{V_0^2}{D^2}\ \text{Kgm.} \quad (22$$

Curves representing the thrust (F_0) as function of I are shown in Fig. 6 for accelerating voltages of 5, 10 and 20 KV. The effective thrust (F_d) of the diode ca also be calculated by means of equations (19), (20) an (22). F_d is also shown in Fig. 6 in comparison with th curves for F_0 vs. D. The power of the diode assumin uniform potential across the beam can be expressed as (using Eqns. 11 and 12)

$$W_0 = IV = P_iV^{5/2} = 1.72 \times 10^{-7}\frac{V_0^{5/2}}{A^{\frac{1}{2}}D^2}\ \text{Watts} \quad (23$$

Combining equations (15), (17) and (23) the effectiv

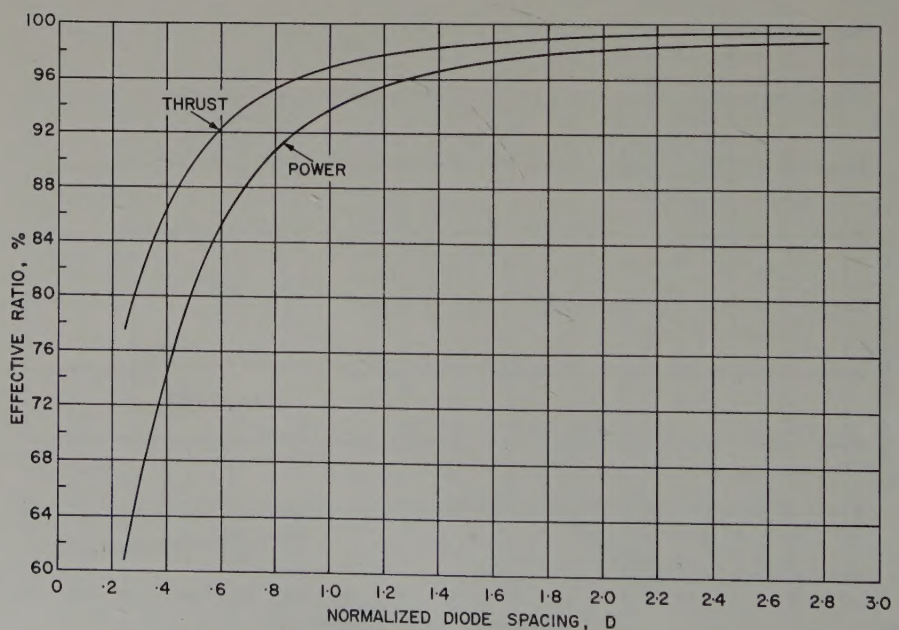


FIG. 5. Effective power and thrust ratios of the ionic diode as function of the normalized diode spacing

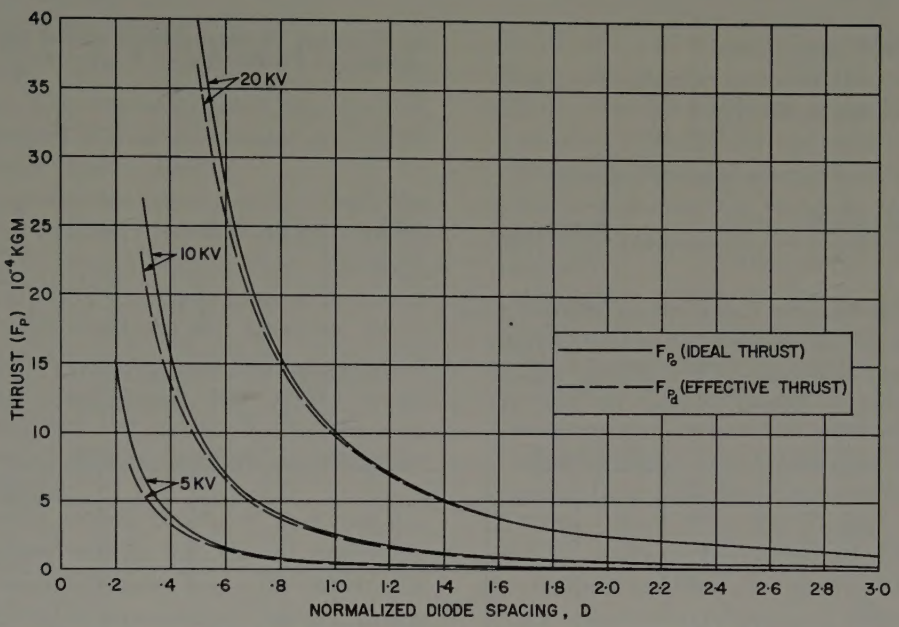


FIG. 6. Ideal and effective thrust of the ionic diode as function of the normalized diode spacing (for cesium ions)

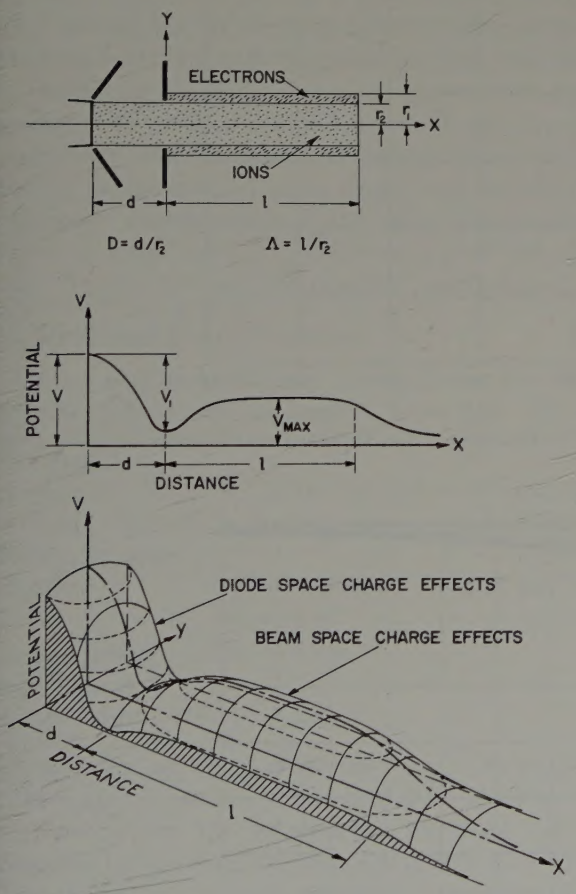


FIG. 7. Sketch of the potential variation in an ionic (diode) rocket.

power may be obtained as function of D; curves similar to the ones for the thrust of the ion diode are then obtained.

2. Effect of the image force due to incomplete charge mixing

To estimate the efficiency of the diode as a thrust device in free-space, it is necessary to take into account the reduction of thrust due to the electrostatic force exerted on the diode by the partially neutralized ion beam. In view of the results obtained above, the overall distribution of potential in the system can be qualitatively represented by sketches of Fig. 7. In addition to the loss of energy within the diode due to the space charge, the ions suffer another loss of energy outside the diode due to the electrostatic force between the incompletely neutralized ion beam and the diode itself. Since the problem is treated as an electrostatic one, the value of the potential in the ion beam outside the diode represents the energy necessary to keep the ions in the configuration assumed at the origin of the problem. The maximum height of the electrostatic "hill" can be expressed in terms of the plane diode parameters.

As a result of Eqn. (3) and Fig. 1, the maximum value of the potential function in the case of concentric cylinders of opposite charge can be expressed as:

$$V_M = \frac{q_\Lambda}{4\pi\epsilon_0} f(\Lambda) \tag{24}$$

where q_Λ is the ion charge per unit length before neutralization

$f(\Lambda)$ is the maximum value of the potential curves (Fig. 1) for a given neutralizing distance.

Values of $f(\Lambda)$ have been calculated for $\Lambda = 30, 6, 3, 1.5, 0.9$ and 0.3. The resulting curve is shown in Fig. 8. Since

$$q_\Lambda = I/v$$

and

$$I = P_i V_0^{3/2}, \qquad v = \left(\frac{2e}{M}\right)^{\frac{1}{2}} V_0^{\frac{1}{2}}$$

for the *ideal* plane diode, the expression for q_Λ in terms of the plane diode normalized spacing becomes, using

Eqns. (11) and (12):

$$q_\Lambda = 7.35 \times 10^{-6} \left(\frac{m}{2e}\right)^{\frac{1}{2}} \frac{V_0}{D_2} \tag{25}$$

Substituting this value of q_Λ into Eqn. (24) gives

$$\frac{V_M}{V_0} = \frac{7.35 \times 10^{-6}}{4\pi\epsilon_0} \left(\frac{m}{2e}\right)^{\frac{1}{2}} \cdot \frac{f(\Lambda)}{D_2} = 0.111 \frac{f(\Lambda)}{D_2} \tag{26}$$

The effective exit power and thrust ratios (relative to the ideal diode) due to the image force of the partially neutralized beam may be expressed in a manner similar to that of the preceding section (Eqns. 15 and 19).

$$\text{Effective Power Ratio} = \eta_{W_e} = \frac{W_e}{W_0} \frac{V_0 - \bar{V}}{V_0} \tag{27}$$

$$= 1 - \frac{\bar{V}}{V_0} = 1 - 0.657 \frac{V_M}{V_0}$$

$$\text{Effective Thrust Ratio} = \eta_{F_e} = \frac{W_e}{W_0} \tag{28}$$

$$= \left(1 - \frac{\bar{V}}{V_0}\right)^{\frac{1}{2}} = \left(1 - 0.657 \frac{V_M}{V_0}\right)^{\frac{1}{2}}$$

By means of the function $f(\Lambda)$ (Fig. 8) and the valu of V_M (Eqn. 26), the effective thrust ratio η_{F_e} ha

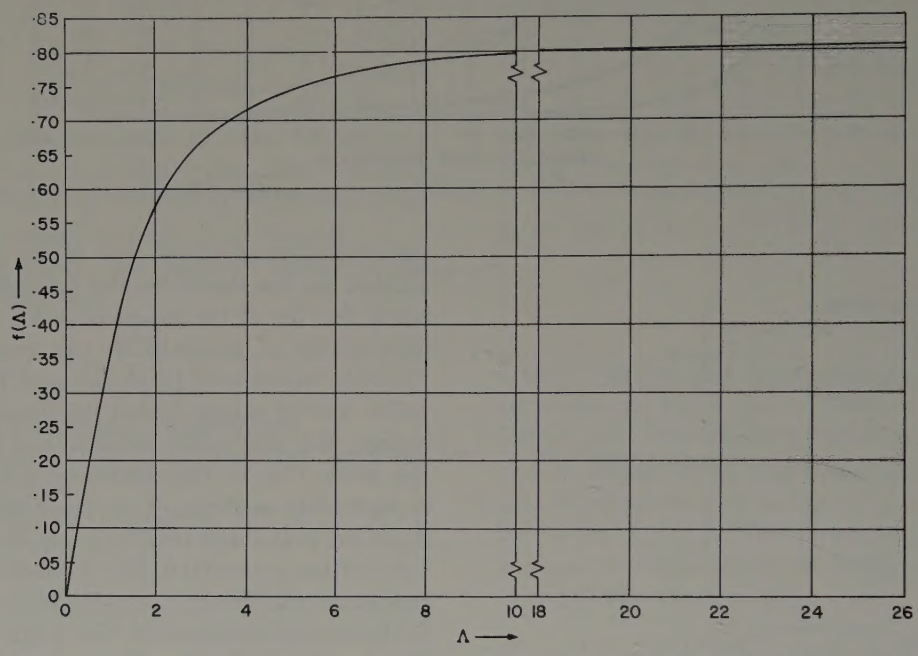


FIG. 8. Variation of the maximum potential on the axis of the ion beam as function of the neutralizing distance (uniform charg distribution).

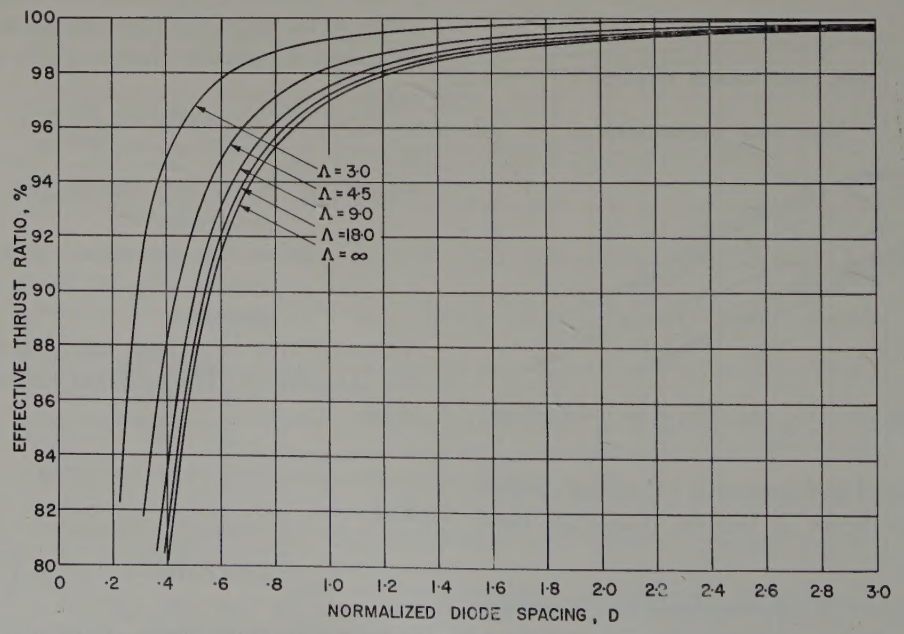


FIG. 9. Effective thrust ratio of the ionic diode as function of the normalized diode spacing for various values of the neutralizi distance.

been plotted in Fig. 9 has function of D for various values of Λ.

As seen from Fig. 9 no improvement in the effective thrust ratio is expected unless the charges are mixed very quickly, i.e. for Λ smaller than 10.

For velocities at which the ions are ejected from the diode, it seems very unlikely that the charges can be mixed or recombined within such a short distance. For example a beam of 0.5 cm. radius has to be mixed within 5 cm. ($\Lambda = 10$) from the exit aperture. For a 6.8 KV beam of cesium ions this distance correspond to an unrealistically short mixing time of 0.15 μsec.

For practical purposes the model of the two long concentric cylinders of charge therefore represents an adequate approximation.

It is seen from the curves of Fig. 9 that the undesirable electrostatic action of the incompletely neutralized ion beam becomes negligible when the diode spacing is allowed to become large (low perveance, low space charge, low mass flow rate). However, from the results presented in Fig. 6 it is observed that the diode spacing has to be made as small as possible for obtaining useful mass flow and thrust from the diode. It appears that a diode perveance corresponding to a spacing D between 0.5 and 1.0 would give the best compromise. For values of D smaller than 0.5, the effective thrust ratio (Fig. 9) drops very rapidly, due to excessive charge effects. If the value of D is allowed to become larger than 1.0, the actual power and thrust would become too low for practical applications.

III. Practical Considerations

A numerical example may illustrate the use of the formulae. The given parameters from Ref. (3) are:

Ion Current Density:	$J = 10$ ma/cm^2	$= 10^2$ Amp/m^2
Ion Beam Radius:	$r_1 = 0.75$ cm	$= 7.5 \times 10^{-3}$ m
Electron Injector Radius:	$r_2 = 0.5$ cm	$= 5 \times 10^{-3}$ m
or	$R_0 = 1.5$	
Applied Voltage:	$V_0 = 6.8$ KV	
Singly Charged Cesium Ion:	$A = 133$	

Potential at the centre of the ion beam. The potential at the centre of the ion beam ($R = 0$) with respect to the potential on the accelerating electrode may be calculated by inserting the above data into Eqn. (7).

For the case $\gamma = 0$, i.e. maximum depression of the electronic charge density, the potential drop is 925 Volts.

For the case $\gamma = 1$, i.e. uniform electronic charge density the potential depression is 572 Volts.

Stuhlinger and Seitz (3) have studied the motion of an electron injected at a given distance from the axis of an infinitely long ion beam. They have estimated the energy of the electron on the axis of the beam by correcting for the average time spent by the electron within the ion beam. Using Stuhlinger and Seitz's theory, the effective value of the potential drop at the centre of the ion beam for this case is (after correction of an error in Stuhlinger and Seitz's formula) 820 Volts.

It is found that by solving Eqn. (7) for $R = 0$, their value corresponds to a parabolic electron density with the electron density at the centre 0.185 times the edge density.

Equivalent value of D. By means of equations (10), (11) and (12) an equivalent value of D may be calculated for the numerical example given above. D is found to be 1.03 which represents the upper limit for the optimum choice of this parameter.

Characteristics for a typical ionic rocket. For a diode spacing D of 1.03, the effective thrust of the diode is 2×10^{-4} Kgm (See Fig. 6). The reduction of thrust and power due to the electrostatic action of the partially neutralized ion beam is only 3% and 6% respectively. For a rocket system weighing 1000 Kgm and having a specific weight of 10 Kgm/Kw (just practical at present without payload) it would be necessary to use 1000 diodes of this type to obtain a thrust of 2×10^{-1} Kgm giving to the vehicle an initial acceleration of 2×10^{-4} g.

Initial condition of charge mixing. In the above analysis it was assumed that the electron distribution through the beam was established immediately at the origin (diode accelerating electrode). The validity of this approximation may be tested by computing the time taken by an electron to reach the centre of the beam. This can be done using Stuhlinger and Seitz's theory and a value of 6.95×10^{-10} sec is obtained for the set of data given above.

For a velocity of 100 Km/sec (6.8 KV) along the axis of the beam, the cesium ions travel only 7×10^{-3} cm before the electrons reach the centre of the beam. Therefore the electron distribution across the ion beam takes place effectively at the exit aperture of the diode.

Beam Spreading. In the above analysis, it has been assumed that the ions move parallel to the axis of the system. In fact, it is well known that due to the space charge forces the ion beam will spread out. The spreading of the ion beam will have the effect of reducing the thrust of the diode if the ions and electrons are not completely mixed prior to a distance for which the divergence of the beam is too large.

Since the thrust will vary as the cosine of the angle of divergence, a large spreading of the ion beam may be tolerated before an appreciable reduction of thrust is obtained. For a beam divergence of 30° the thrust at the edge of the beam will be reduced by 13% of its value if no spreading were occurring. The overall reduction of thrust should be even smaller since the angle of divergence for the ions within the beam is less than for the ions at the edge; for a uniform distribution the overall decrease is 11%. Furthermore the beam spreading is likely to facilitate the mixing of electrons and ions, and consequently should tend to reduce the image force of the ion beam.

Recombination and mixing distance. It was found, in the above example, that the electron energy at the centre of the ion beam is in the range of 600 to 900 eV. Therefore at the beginning of the mixing process the beam will effectively behave like a hot plasma in which the electrons will lose their energy mostly through inelastic collisions with the ions. Dandurand and Holt (4) have reported a value ($\alpha_{Cs} = 10^{-7}$ cm^3/ion-sec) for the recombination coefficient between electrons and ions in the afterglow of a cesium discharge (about 1 electron volt energy). The electrons in the plasma from an ionic rocket would be much faster (hundreds of electron volts) than those for which Dandurand and Holt obtained their value for α_{Cs}. For the above numerical example, the ion density is 6.25×10^9 ions/cm^3 and the recombination time is 1.6 milliseconds for slow electrons and much longer for fast electrons. A beam of 6.8 KV cesium ions will travel 0.16 Km, during that period, and recombination would have only just begun.

It is not essential, however, that the ions and electrons be completely recombined since as soon as the ions and electrons are being mixed, the electrostatic potential within the beam will decrease. This situation is illustrated in Fig. 3 where the potential on the axis of the beam is plotted for various values of the ratio (R_0) of the radii of the electron and ion beams. This ratio R_0 can be considered as a measure of the amount of mixing between ions and electrons. The curves of Fig. 3 also indicate that there is a definite advantage o injecting the electrons as closely as possible to the ion beam.

Conclusion

As long as the overall neutrality of the ionic rocke exhaust is preserved, complete charge mixing and/o recombination further than a distance of ten bean radii has little effect on the system. Thus only charg separation near the rocket affects the performance.

It has been found that an electrode spacing betwee 0.5 and 1 times the ion beam radius represents th optimum range of operation of an ideal plane diode a a thrust device. Above this range the mass flow rat and the thrust are too low for practical applications For a spacing below this range the space charge effect limit the performance of an ionic diode quite sharply.

This work was supported by Astro-Electronic Prod uct Division of Radio Corporation of America Princeton, New Jersey.

References

1. Smith, L. P. and Hartman, P. L., J.A.P. **11,** 220 (1940).
2. Pierce, J. R., "Theory and Design of Electron Beams, D VanNostrand Co. Ltd., N.Y. (1949) P. 161.
3. Stuhlinger, E. and Seitz, R., I.R.E. Trans. PGME, 3 27 (1959).
4. Dandurand, P. and Holt, R. B., Phys. Rev. **82,** 278 (1951)

Ephemeris Time

T. P. Gabbard*

Abstract

Ephemeris Time is defined and its meaning briefly discussed; following this is a historical development of the events leading to the recognition of Ephemeris Time as a successor to Universal Time for use in precise work. The determination of Ephemeris Time utilizing lunar datum and atomic and/or molecular clocks is delineated, and some uses of the more uniform time measure are indicated.

1. Introduction

Man has long been concerned with time, for it has regulated his life from his first dawn. Time is the subject of this paper; and in particular, man's latest achievement in denoting the uniform passage of this fleeting dimension—Ephemeris Time (ET). The pattern will be to discuss, in turn, the meaning, history, measurement and uses of ET; and since the "meaning" of time is more properly a subject for philosophy, this area will be touched but lightly. Stress will be placed primarily upon the history, most recent methods of accurate time determination and some uses to which this increased accuracy may be profitably directed.

* Hughes Aircraft Company, Culver City, California

2. Meaning and Definition of Ephemeris Time

As to the origin of the name "Ephemeris Time," ET is derived from it being the independent variabl in the ephemerides, or time schedules, of celestia bodies; it is perfectly uniform in passage and is ofte used interchangeably with the name Newtonian time In Newtonian mechanics, time is looked upon a being instantaneously the same through the whole o space—a "now" which is present everywhere but i inexorably passing into a new.

This view of time is to be contrasted with that a presented by relativity theory. Here, there is n longer the dichotomy of space and time, but rathe the concept of a space-time continuum. Time is n longer unconditionally the same for two observe through all space, but is dependent not only upon th relative positions of the observers, but also thei relative velocity. However, time will become New

tonian for two observers if the relative velocity between them becomes zero and will be essentially so for small relative velocities.

It is enlightening to look upon Newton's First Law of Motion (the Law of Inertia) as defining equal intervals of time, i.e. uniform time. Paraphrasing the Law of Inertia, "Two intervals of time are equal by definition if a body subject to no forces moves over equal distances in them." It is in this sense that we have so far used ET; however, let us look at a more practical, working definition of ET.

At the September 1955 meeting of the International Astronomical Union (IAU) in Dublin, the IAU adopted ET as the measure of time to be used in precise work and, further, defined the unit of ET, the ephemeris second, as 1/31,556,925.975 of the tropical year 1900.0 (1). ET is related to Universal Time (UT) by the equations $ET = UT + \Delta T$ and $\Delta T = 1.821\ \Delta L'_M$, where $\Delta L'_M$ is the difference between the observed mean longitude of the Moon and the value tabulated in the new lunar ephemeris (*Improved Lunar Ephemeris 1952–1959*). These equations will be considered as defining ET.

3. Historical Developments Leading to the Recognition of Ephemeris Time

Before going further, it will be rewarding to look at the historical developments leading to so unique, singular a definition of the ephemeris second and to the relationship of ET and UT described. It will be further noted that there is a contending unit of time measurement[1] afforded by the atomic clocks developed in recent years; and it will be seen that these two basically different units of time[2] and the methods of determining them combine to give man his most accurate means ever for time determination.

Data accumulated over several centuries point out the departures of the Moon, Sun and planets from their positions predicted from gravitational theory. It was noted early that the Moon's motion had a secular component of acceleration; from records of eclipse studies, Halley concluded in 1695 that the motion of the Moon was being accelerated (2). It was later shown that a term of approximately $10''T^2$ (T in centuries) had to be applied to the mean longitude of the Moon to account for the acceleration; however, approximately half of the above term has been shown to be attributable to perturbative influences of the other planets on the Earth-Moon system.

In 1927, de Sitter found, from a study of lunar and solar eclipse records covering about two thousand years, that the Moon's secular acceleration (not accounted for by gravitational theory) in mean longitude amounted to $+5.22'' \pm 0.30''$ per century per century (3). It was further noted by Cowell in 1905 that there was also a secular acceleration of the Sun's motion (2). de Sitter's value for the Sun's acceleration is $+ 1.80'' \pm 0.16''$. These secular accelerations have come to be attributed to the slowing of the Earth's rotation due to tidal friction.

In addition to the secular variation mentioned, Newcomb, in 1870, found that there were also irregular, possibly long period, fluctuations in the Moon's motion which could not be accounted for by the current tables of the Moon (Hansen's Tables: published 1857) (2). Newcomb accounted for the fluctuations through the introduction of a theoretically unsubstantiated, empirical term which has become known as the Great Empirical Term.

Irregular fluctuations in the Sun's and planets' motions were not recognized until after Brown (5) developed his lunar theory and constructed his Tables of the Moon. In the construction of his Tables (1919), Brown incorporated the Great Empirical Term and the secular acceleration term due to planetary pertubations, but he did not include the secular term due to tidal friction. Through the use of the fluctuation of the Moon, B, Spencer Jones was able to show in 1939 that the observed departure from prediction of the Sun from Newcomb's Tables (6) is expressible in the form $\Delta L_S = + 1.00'' + 2.97''T + 1.23''T^2 + 0.0747B$ (7); here, T is measured in Julian centuries from Greenwich Mean Noon 1900.0 (January 0.5 UT), and the time of observation is in UT units. B is defined as the fluctuation in the Moon's longitude and is the difference between the observed mean longitude of the Moon and the tabular value from Brown's Tables. Similar expressions may be derived for the several planets, where the secular and irregular terms are proportional to the mean motions of the planets.

In the expression above, the first two terms are for adjustment to the epoch 1900.0. The third term represents the secular acceleration due to tidal friction slowing the Earth; however, note that the value is found to be different from the 1.80″ value of de Sitter. The fourth term is the irregular acceleration which is due to irregular fluctuations in the Earth's rotation rate. It may at first sight appear strange that data from an observation of the Moon (B) would appear in the ΔL expressions of the Sun and planets. However, it must be remembered that we cannot detect the Earth's fluctuations in rotation by purely terrestrial data—we must look to the celestial bodies for a "reflection" of these fluctuations in rotation rate. The "reflection" from the Moon is greatest, easiest measured and thus is used as the yardstick for the irregular fluctuations in the Earth's rotation rate.

It will be remembered that when UT was first instituted, it was thought to be Newtonian in character; hence, it was thought that comparison of observed positions as functions of UT, and tabular positions, as functions of a perfectly Newtonian time (ET), for

[1] The atomic time unit has been termed the "essen" by G. M. Clemence (4).

[2] The ephemeris second is of an astronomical nature and based upon gravitation, whereas the essen is of a physical nature and based upon atomic processes.

celestial bodies would give zero residuals—except for uncertainties in constants, imperfections in gravitational theory and observational errors.

As we have noted, the residuals are non-zero and are composed of secular and irregular components. Since the components of the residuals for the several planets are proportional to their mean motions, it is seen that the source of the residuals is most logically and rightfully assigned to the inconstancy of UT or as has been said, the inconstancy of the Earth's rotation rate—since UT is measured by the rotation rate of the Earth. Had NEWCOMB's Tables been entered with the time of observation in ET units, ΔL_S would have been zero; thus, the ΔL_S is attributable to the difference in ET and UT. Where K = 24ṣ349/1.00″ and is a measure of the rate at which the Sun's mean longitude increases, we see that ET − UT = ΔT = K ΔL_S, or ΔT = + 24ṣ349 + 72ṣ3165T + 29ṣ949T² + 1.821B. As before, the third and fourth terms represent, respectively, the secular and irregular components, and the first two terms are for adjustment to the epoch 1900.0. Hence, for the year 1900.0 (T = 0) ET = UT, in epoch and duration. To explain the source of the definition of the ephemeris second given earlier, we first note that the unit of UT is the mean solar second and is 1/86,400 of a mean solar day; hence, the number of mean solar seconds in the tropical year 1900.0 is 86,400 times the tropical year 1900.0 in mean solar days and is 31,556,925.975 seconds. Since ET = UT for the year 1900.0, the ephemeris second is equal to the mean solar second for that time, i.e. the ephemeris second is the fraction 1/31,556,925.975 of the tropical[3] year 1900.0.

We have seen that ET − UT = ΔT, or ET = UT + ΔT. It remains to show that ΔT = 1.821 $\Delta L'_M$. SPENCER JONES has shown that the observed departure from prediction in mean longitude of the Moon from BROWN's Tables is expressible in the form ΔL_M = + 4.65″ + 12.96″T + 5.22″T² + B − Empirical Term (7). Here again the time of observation is in UT and T is in Julian centuries reckoned from the epoch 1900.0. Note that DE SITTER'S 5.22″ value is retained for the secular component. Where K′ = 1″/1ṣ821 and is the rate at which the Moon's mean longitude increases, the Moon will increase its mean longitude by K′ ΔT in the interval ΔT; hence, the Moon's increase in mean longitude in time ΔT is $\Delta L_{M(\Delta T)}$ = K′ ΔT = + 13.37″ + 39.71″T + 16.44″T² + B.

Thus, when the time of observation is referred to ET, the correction to BROWN's Tables becomes ΔL_M − $\Delta L_{M(\Delta T)}$ = − 8.72″ − 26.75″T − 11.22″T² − Empirical Term. It is principally through the inclusion of this corrective term that BROWN'S *Tables of the Motion of the Moon* becomes the *Improved Lunar Ephemeris 1952–1959* (ILE). The effect has been to enter into the lunar theory the same unit of Newtonian time as used for the theories of the Sun and planets.

If now, the time of an observation in ET units is taken into the ILE, there will be no difference in observed and tabular values of mean longitude—except, again, that due to uncertainties in constants, imperfections in theory and observational error. However, if the time of observation in UT units is taken into the ILE, there will be found an error $\Delta L'_M$ in the observed and tabulated mean longitude which will be due to the difference in ET and UT for the epoch of the observation. Hence, ET − UT = ΔT = (1/K′) $\Delta L'_M$ = 1.821 $\Delta L'_M$.

We have briefly seen the necessity of the transition from UT to ET and the essence of the principle of the conversion of the one to the other; however, in going from UT to ET we have given up a relatively accessible, variable time for a relatively inaccessible, invariable one. CLEMENCE (4) has indicated that, within a year, the year can be determined with a probable error of 1 part in 10^{10} in UT units by astronomical methods using the Photographic Zenith Tube (PZT); however, to obtain the same accuracy in ET units, five years of observation would be necessary. Probable errors of the order of 1 part in 10^9 in ET units is expected from a single year of observation.

In recent years, however, there have been developed atomic clocks which equal, if not exceed, the accuracy of time determination by astronomical methods—but without the lengthy delay. In 1955, ESSEN and PARRY (8) announced that they had achieved an accuracy of 1 part in 10^9 in time and frequency[4] determination derived from atomic processes and employing magnetic resonance techniques. There is thus available a new standard of frequency for calibration of other frequencies which permits of the same accuracy in a few minutes as given previously by astronomical methods requiring a period of a year.

In the light of the ESSEN-PARRY article, BULLARD (9) suggested that the astronomical second (ephemeris second) be abandoned in favor of a 'physical second' (essen) for the most refined experiments. With reference to the BULLARD article, the IAU defined the unit of ET as previously stated.

4. The Determination of Ephemeris Time

Further response to the BULLARD article came from CLEMENCE (10). Among other things, he pointed out that the atomic standard clocks could not establish an epoch. Astronomical observations of celestial bodies will be made to establish an epoch, and their motions will define the primary standard of time. The atomic clocks will serve as secondary standards to mark the passage of time between epoch determination—just as the quartz crystal clocks (and earlier still, mechanical clocks) have done in the past.

[3] The sidereal year was first proposed, but it was later replaced by the tropical year which requires no knowledge of the constant of precession and is thus more accurately known.

[4] Frequency is here used in the sense of the ratio of time intervals.

We have noted that there is a long period measurement of ET using astronomical methods and a short period determination using atomic clocks. Taking these methods in turn, we remember that ET = UT + ΔT. UT is determined from observation using the PZT and ΔT is determined from observation using the Markowitz dual-rate Moon position camera.

4.1. Long-Term Determination of Ephemeris Time

4.1.1. *Determination of Universal Time* (UT). The PZT was devised by Ross (11) primarily to determine variations in latitude. The first was installed for its stated purpose in 1915. In 1933, it was adapted for the determination of UT and eventually replaced the transit instruments for this purpose. The PZT is directed toward the zenith[5] so that only those stars passing on or near the zenith will be photographed. The upper element of the instrument is called the rotary and contains the lens, photographic plate holder and drive mechanism. Light passing through the lens continues on through a fixed vertical tube until it is reflected by a basin of mercury situated separate from and below the tube. The light is reflected from the pool of mercury back along the tube to the rotary where it is brought to focus on the photographic plate.

Littell and Willis (12) have described two possible methods of using the PZT for time determination: one method permits the stars to trail and the other provides drive to the plate holder permitting point images to be formed. Littell (13) later found the latter method to be best. In somewhat more detail, this method is as follows: The plate drive mechanism moves the photographic plate in a west-east direction sufficient to balance the Earth's rotational motion. Before transit, three, fifteen-second exposures of the star are made. To permit this, the photographic plate is moved approximately 0.01 inch in the north-south direction between exposures. About five seconds before transit, the rotary is rotated 180 degrees; and starting about five seconds after rotation, there are formed three more fifteen-second exposures.

Associated with each of the six star images are approximately twenty-seven time records, or eighty-one pairs total. Any pair, one before and one after rotation, would give the time of transit in units of clock time; but in practice, several pairs (a dozen or so) are used to obtain a more accurate value. Necessary correction to clock time for obtaining UT is determined from ephemeris data of the observed star's right ascension for the date and the right ascension of the mean Sun for the epoch of observation. During a night's observing, some fifteen to twenty stars are photographed, giving a probable error of about three milliseconds (4) in the mean result of mean solar time (UT) so determined. This method, over a period of a year, will give the accuracy previously stated of 1 part in 10^{10}.

[5] It will be noted that, the PZT being a zenith instrument, the effect of atmospheric refraction will be minimal.

4.1.2. *Determination of* ΔT. In determining ET, ΔT must also be known in addition to UT. To determine ΔT, observations of the Moon's actual position must be compared with its position given in the ILE; however, its actual position at a well-defined epoch is difficult to obtain using conventional techniques. The Moon's greater brilliance in relation to the comparison stars results in an irradiation effect which makes the limb difficult to determine, and the Moon's motion in the background of stars during the length of exposure creates an elongated lunar image whose center is difficult to ascertain. In addition to these difficulties, there is the further lack of a well-defined epoch for the observation.

To overcome these difficulties, Markowitz (14) developed the dual-rate Moon position camera; the camera went into use at the U.S. Naval Observatory in 1952. To eliminate the irradiation effect, the Moon's image is intercepted by a plane, plate filter 1.8 mm thick which has a transmission factor of 0.001. A second, yellow filter having a hole in its center,[6] is located behind the first and is situated on the plate holder mechanism; its purpose is to cut out the blue rays of the stars.

Normal tracking on the stars is not accomplished by the telescope drive, but rather the telescope is stationary and the camera's plate holder is driven in right ascension to permit tracking on the stars. To eliminate the effect of an elongated lunar image, the lunar filter is tilted at a rate which maintains the Moon's image fixed in the background of stars. When the filters are parallel, the lunar filter passes the Moon's rays undeviated; and at the instant the filters are parallel, a set of electrical contacts close to mark the epoch of the observation—in UT units.

Reduction of the plate (14, 15) is as follows: Coordinates of 30–40 points on the Moon's bright limb and about 10 comparison stars are obtained with a two-screw measuring engine. Since only three positions on the limb would be sufficient to define the center of the Moon, the method of least squares must be used when so large a number as 30–40 are used. The result is, then, the Moon's center of figure given in right ascension and declination for the epoch of the observation.

At this time, it is to be noted that, in practice, ΔT is not determined from $\Delta T = 1.821\ \Delta L'_M$; but rather, by the method outlined in the ILE (16). Here, the value of right ascension of the Moon's position is taken into the ILE and the value of ET is read out for which the value corresponds. This, then, is the epoch of the observation in ET units. The difference ET$-$UT for the epoch of the observation is ΔT. ΔT can also be determined using the declination, but it is not expected, however, that the two values agree exactly. The final, accepted value is obtained from an averaging of the

[6] The hole in the center of the second filter is to permit the Moon's rays from the first filter to strike the photographic plate without further diminution.

two. A more accurate value of ΔT is obtained if the coordinates of the center of figure are first converted into those for the center of mass before entering the tables.

From one observing station, ΔT should be determined, over one lunation, with a probable error of 0s1 (15), and from observations over a period of one year, should determine absolute frequency to 3 parts in 10^9. About twenty dual-rate cameras were scheduled for operation throughout the world during the recent IGY; four are planned to be maintained in continued operation afterward. It was with consideration of four in operation that the value, previously given, of 1 part in 10^9, over a period of a year, was given.

4.2. Short-Term Determination of Ephemeris Time

We have seen how man has gone from a time determination employing the Earth's rotation as a measure to one employing, essentially, the Earth's revolution about the Sun. In all times though, it has been necessary to use the most accurately available Earth-bound timepiece for extrapolation between astronomical time determinations; however, these have been considered inferior timepieces, until quite recently, to the natural periodicity afforded by the celestial bodies and are daily checked upon, weather permitting.

It is not to be overlooked, however, that there are advancements in the construction of more accurate time pieces; from the pendulum devices through the quartz crystal oscillators, we have arrived at the family of atomic clocks. We will look briefly at the ammonia, cesium and maser type clocks.

4.2.1. *Ammonia and Cesium Clocks: Resonance Absorption Techniques.* Fundamental to the ammonia and cesium type clocks, however, is the quartz crystal clock. Quartz is a piezoelectric crystal, and when properly cut and placed in a suitable oscillator circuit becomes a source of relatively stable electric oscillations. A representative value of these oscillations may be, say, 100,000 cycles per second (cps). These oscillations are then counted-down through several cascaded multivibrator stages to a nominal value of 1,000 cps or, possibly, 60 cps. Here they undergo a few stages of power amplification and eventually drive what may be an ordinary electric clock. The fundamental oscillations could as well have undergone frequency multiplication and amplification and eventually been broadcast as radio signals. However, a drawback to the quartz clock is a secular change in frequency with age.

The ammonia (17, 18) and cesium (8, 17) clocks are similar in that they provide a means for stabilizing the frequency of the quartz oscillator by comparison to an atomic or molecular standard of frequency. The method of comparison is one of resonance absorption. In the case of the ammonia molecule, the frequency of absorption used for comparison arises from the nitrogen atom oscillating between its two possible positions with respect to the three hydrogen atoms. The three hydrogen atoms form the base of a triangular pyramid whose apex is occupied by the nitrogen atom; however the nitrogen atom can oscillate "through" the base to a second possible apex.

For cesium, which is an alkali metal and hence hydrogen like in structure, the absorption frequency arises much as does the 21 cm absorption of the neutral hydrogen atom. The spin of the outermost, valence electron can be either parallel or antiparallel to the nuclear spin, giving rise to two distinct energy states of the cesium atom. In the case of the cesium atom, the frequency of absorption used for comparison arises from the difference of energy of these two states.

In both the ammonia and cesium clocks, quartz crystal oscillations are multiplied in frequency until they are equal to the resonance absorption frequency of the atomic standard. Then, in the ammonia clock, the signal is applied to one end of a waveguide filled with ammonia gas. At the farther end of the waveguide is a microwave detector. If the input to the detector is not a minimum (absorption in the waveguide a maximum), the detector output will alter the quartz crystal oscillator frequency until it is a minimum.

In the cesium clock, the method is somewhat different. Here, the multiplied oscillator output reacts with a beam of cesium atoms to effect absorption of the microwave energy; the effect of the absorbed energy on the beam is to increase the number of the cesium atoms in the higher of the two energy states discussed. After reaction with the microwave energy, the beam of cesium atoms passes through a magnetic field which isolates the atoms in the different energy states and permits those atoms in the higher energy state to continue on to a detector. If the detector output current is not maximal, the crystal oscillator frequency will be shifted until it is.

4.2.2. *Maser Clock.* The maser (18, 19) differs from the ammonia and cesium clocks primarily in that it does not depend upon the mechanism of absorption. Instead, the frequency standard of the atom itself is used directly—much as the initial crystal oscillations of the quartz clock had been. The maser can use any of several different atomic or molecular sources; but, for illustration, we will consider only the use of the cesium atom.

In a group of cesium atoms, there will be some atoms in each energy state previously discussed. Forming the atoms into a beam and passing them through a magnetic field (as was done in the cesium clock), a beam can be generated which is predominantly made up of atoms in the higher of the two energy states. If such a beam, of sufficient intensity, is fed into a resonant cavity of the proper dimensions,[7] the cesium atoms will return to the lower energy state and give up their energy to the cavity. The cavity oscillations are then

[7] The dimensions of the cavity are such that it is resonant to the frequency of oscillation given off by the atoms when returning to the lower energy state.

coupled out by means of a waveguide to the amplifying and count-down circuits. If a beam of intensity insufficient to sustain oscillations in the cavity is present, an input signal frequency equal to the cavity frequency will stimulate the cesium atoms to radiate, with the result that the input signal frequency appears increased, or amplified. This is the principle of the maser[8] as an amplifier.

The accuracy of the ammonia and cesium clocks are dependent upon the sharpness of the associated absorption curve; the cesium clock overcomes the Doppler broadening which is inherent in the ammonia clock and is thus the more accurate of the two. It was using a cesium clock that Essen and Parry (8) achieved their epoch-making frequency determination. The maser presently holds the highest hopes for the greatest accuracy; it is anticipated that the maser may achieve an accuracy of 1 part in 10^{13} when using the cesium atom (17).

5. Some Uses of Ephemeris Time

When speaking of the "uses" of an improved unit of time, one is faced with an enormous problem of selection; for in all scientific and technical areas of human endeavor, a more precise, uniform standard of time determination will find immediate use—if for only pushing the value of some constant out to another significant figure. But it is just this knowledge of the added figure that may open a new corridor into the unknown.

In astronomy, an effect of the use of the new time (ET) has been the removal of a glaring inconsistency between lunar theory and planetary theory—they now use the same time variable in the ephemerides. If now, unaccounted-for errors exist between observation and theory for the position of the Moon, Sun and planets, there leads a way to improved gravitational theory. Discrepancies may indicate necessary revision to orbit parameters or masses; in general, the new time should permit improvement in both lunar and planetary theory.

The physicist and radio engineer will use the new time unit for expressing frequency much as previously but to a higher accuracy. Where f_U is the frequency based on UT units, f_E is the frequency based on ET units and D ΔT is the change per annum of ΔT, $f_E = f_U(1 - D\ \Delta T/31{,}556{,}925.975) = f_U(1 - 3.1689 \times 10^{-8} D\Delta T)$ (1). f_U is determined by comparison to the national time services radio broadcasts and the D ΔT is published regularly by the time services. Once the f_E of the atomic frequency standard (e.g., the absorption frequency of the ammonia and cesium clocks) has been sufficiently accurately determined, ET may be broadcast directly by the time services.

This (the determination of the essen in ET units) leads to one of the most fundamental questions which may be answered by the new time measures: Is the ephemeris second and the essen measuring the same, or, is the time from gravitational measurements the same as that from atomic measurements? In kinematic relativity (4, 9), there are two natural time scales present, which do not keep in step. Milne, Dirac and others have suggested they be associated with atomic and astronomic frequencies. A much looked-for result is the manner in which the essen and ephemeris second keep in step. As has been often and aptly said, 'Time will tell'—the answer to this question and many more.

[8] Maser is a shortened expression for microwave amplification by stimulated emission of radiation.

References

(1) Jones, H. S., 1955, "Definition of the Second of Time," *Nature*, **176,** 669.

(2) Jones, H. S., 1956, "Non-seasonal Changes in the Earth's Rotation," *Vistas in Astronomy*, 827.

(3) Jones, H. S., 1939, "The Rotation of the Earth, and the Secular Accelerations of the Sun, Moon, and Planets," *Monthly Notices of the Royal Astronomical Society*, **99,** 541.

(4) Clemence, G. M., 1956, "Standards of Time and Frequency," *Science*, **123,** 567.

(5) Brown, E. W., 1919, "Tables of the Motion of the Moon," Yale University Press.

(6) Newcomb, S., 1898, "Tables of the Sun," *Astronomical Papers of the Americae Ephemeris*, Volume VI, Part I.

(7) Clemence, G. M., 1948, "On the System of Astronomical Constants," *Astronomical Journal*, **53,** 169.

(8) Essen, L. and Parry, J. V. L., 1955, "An Atomic Standard of Frequency and Time Interval," *Nature*, **176,** 280.

(9) Bullard, E. G., 1955, "Definition of the Second of Time," *Nature*, **176,** 282.

(10) Clemence, G. M., 1955, "Definition of the Second of Time," *Nature*, **176,** 1230.

(11) Ross, F. E., "Latitude Observation with the Photographic Zenith Tube at Gaithersburg, Md.," Special Publication No. 27, U. S. Coast and Geodetic Survey.

(12) Littell, F. B. and Willis, J. E., 1930, "A New Method of Determining Time," *Astronomical Journal*, **40,** 7.

(13) Littell, F. B., 1934, "Clock Corrections from Observations with the Photographic Zenith Tube," *Astronomical Journal*, **43,** 9.

(14) Markowitz, W., 1954, "Photographic Determination of the Moon's Position and Applications to the Measure of Time, Rotation of the Earth, and Geodesy," *Astronomical Journal*, **59,** 69.

(15) Markowitz, W., 1954, "The Determination of Universal Time and Ephemeris Time at the U. S. Naval Observatory," Congress International de Chronometrie, Paris, 1954, 71.

(16) Improved Lunar Ephemeris, 1952–1959, pg. XII.

(17) Lyons, H., 1957, "Atomic Clocks," *Scientific American*, **196,** 71.

(18) Townes, C. H., 1952, "Microwave Spectroscopy," *American Scientist*, **40,** 270.

(19) Culver, W. H., 1957, "The Maser," *Science*, **126,** 810.

Biological Shielding for Radiation Belt Particles

D. L. Dye* and J. C. Noyes†

Abstract

Calculations are made, for the particle spectra in the most intense regions of the radiation belts, of the attenuation of the particle flux by shielding on a space vehicle, and of the biological dose rate due to the flux which has penetrated the shielding. Both protons and electrons are considered in the inner belt, but only electrons in the outer belt. Secondary particles and bremsstrahlung produced by these particles on interacting with a shield are also considered. It is shown that, despite the much higher electron fluxes, the protons are of much greater biological significance.

Introduction

With the discovery of trapped radiation belts around the earth at altitudes between approximately 1,000 km to 50,000 km, there has arisen the question as to the magnitude of radiation dose that would be received by the occupant of a space vehicle which passed through these regions. In addition, there has been raised the question of the amount of shielding that would be required in a space vehicle to protect the occupant, should the dose rates in the radiation belts prove to be high or the time spent therein long.

It is the purpose of this paper to discuss quantitatively the question of dose rate and effectiveness of shielding in reducing dose rates in the most intense regions of the radiation belts. Estimates are made, based on experimental data, of the particle spectra in these regions. Calculations are then made of the attenuation of incident particle flux due to various amounts of shielding, and of the biological dose rate due to the flux which has penetrated the shielding.

The next four sections are concerned with the inner belt protons, which are known to be the most penetrating particles in the radiation belts, and with the secondary radiation generated by the protons on interacting with a shield. The last two sections are devoted to the electrons in the inner and outer belts, respectively, and to the bremsstrahlung which they produce.

Incident Proton Spectrum

With data now available [1, 2, 3, 4] regarding the flux and energy distribution of the protons of the inner radiation belt, it is possible to make reasonable estimates of the incident radiation intensity above 40 Mev in this region around the earth. Below 40 Mev theoretical forms of the energy spectrum [5] exist based on neutron leakage from the atmosphere. The total omnidirectional flux above 40 Mev has been given by Van Allen [2, 4] as 2×10^4 protons/cm²-sec in the heart of the inner belt. Some doubt [6] exists as to the validity of the Freden and White spectrum [3] over the whole belt region, but it certainly represents an average over that part of the belt through which their emulsions passed, and no better form for this spectrum is yet known.

Figure 1 shows differential energy distributions of inner belt protons which fit the experimental data now known. P_1 is the form given by Hess [5] below 100 Mev, joined to the form $\exp(-E/120)$ above 100 Mev [3], having a total of 2×10^4 protons/cm²-sec above 40 Mev. P_2 is an alternate spectrum which fits the data:

$$P_2(E_i)dE_i = 1.04 \times 10^4 E_i^{-1}\, dE_i (40 < E_i < 100 \text{ Mev}) \quad (1$$

$$P_2(E_i)dE_i = 1.04 \times 10^6 E_i^{-2}\, dE_i (E_i > 100 \text{ Mev})$$

The subscript i refers to incident particles, and capital P refers to the absolute omnidirectional flux distribution. Lower case p is used to designate a spectrum normalized to one incident proton/cm²-sec total flux of energy above 40 Mev. $p_2(E_i)$ is plotted in Figure 2, along with spectra calculated later. By using Van Allen's total flux, $P(E) = 2 \times 10^4 p(E)$. The biological dose calculations reported here are based on the form $p_2(E_i)dE_i$ for the incident spectrum.

Proton Attenuation and Spectrum Degradation

The incident protons impinge upon the outer shell of a vehicle, and are partly absorbed and degraded to a new spectrum by it. It is then assumed that they enter some absorber designed to reduce the dose inside effectively. Polyethylene (CH_2) has here been chosen as the material for this absorber because it effectively stops protons, on a weight basis, as well as or better than most other substances, with a minimum of nuclear reaction products. The radiation entering the vehicle interior, i.e. the astronaut's compartment

* Nuclear Physics Unit, Aero Space Division, Boeing Airplane Company, Seattle, Washington

† Geo-Astrophysics Laboratory, Boeing Scientific Research Laboratories, Boeing Airplane Company, Seattle, Washington

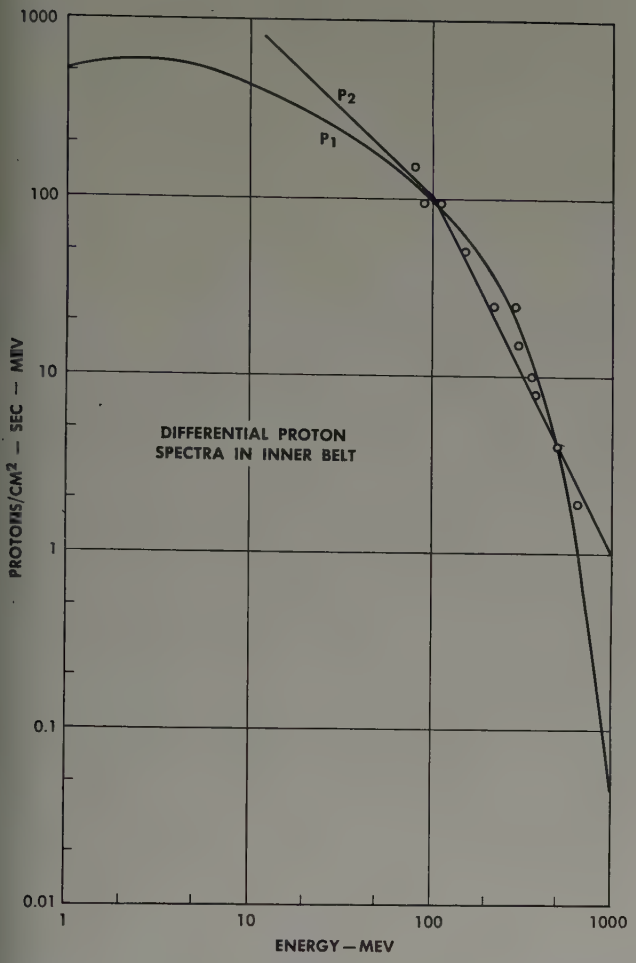


FIG. 1. Inner radiation belt proton differential energy spectra. Circles are the experimental data of Freden and White [3]. P_1 is one of their curves fitting the data. P_2 is the power law spectrum used in this paper, Equation (1).

thus consists of degraded energy incident protons, neutrons and gamma rays generated in the metal shell by (p, n) and (p, γ) reactions, plus penetrating electrons and electron-produced bremsstrahlung. These will be discussed in turn.

Tables of range vs. energy for protons in various materials [7] were used to calculate the energy degradation as the protons pass through matter. Using only $R_z(E)$, range as function of energy in a material Z, one may write:

$$R_z(E_i) = X_z + R_z(E_f) \tag{2}$$

where X_z is the thickness of the absorber Z, and E_f is the final energy of the proton after passing through this thickness. E_i is the incident proton energy.

The form of $R_z(E)$ may be approximated by a power law,

$$R_z(E) = kE^n, \tag{3}$$

where both k and n depend on E as well as (slightly) upon Z. If we denote initial and final energies by subscripts i and f, and consider only a single material, then Equation (1) becomes:

$$k_i E_i^{n_i} = X + k_f E_f^{n_f}. \tag{4}$$

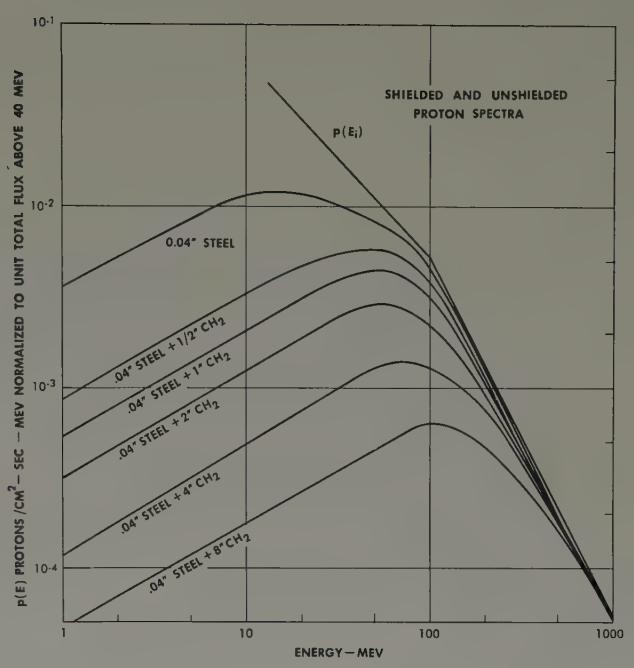


FIG. 2. Proton differential flux spectra, normalized to unit incident flux over 40 Mev. The top curve is the unit incident flux, p_2 (E). The other curves are degraded energy spectra resulting from passage of the incident flux through the indicated shielding.

Differentiating,

$$dE_f = \frac{k_i n_i}{k_f n_f} \frac{E_i^{n_i - 1}}{E_f^{n_f - 1}} dE_i \tag{5}$$

Hence, if $p(E_i)dE_i$ particles enter the absorber having energies in the range E_i to $E_i + dE_i$, where E_i is large enough so that traversal takes place through a thickness X, then this same number will emerge having energies in the range E_f to $E + dE_f$, neglecting straggling. In equation form,

$$p(E_f)\, dE_f = p(E_i)\, dE_i$$

$$= p(E_i) \frac{k_f n_f}{k_i n_i} \frac{E_f^{n_f - 1}}{E_i^{n_i - 1}} dE_f. \tag{6}$$

Over the range of interest here, 40 to 1000 Mev, and for relatively small energy losses in the absorbers, k and n may be considered constants, and the ratio $k_i n_i / k_f n_f$ set equal to one.

In (6) E_f is related to E_i in such a way that (2) is satisfied if X is thin enough so that E_i is not entirely absorbed. This is equivalent to integrating the energy loss rate equation of Bethe-Bloch [7] over the absorber thickness and subtracting it from the original energy.

The recipe for obtaining E_f from E_i and X_z is as follows: for E_i, get $R_z(E_i)$ from the range-energy table, and subtract X_z from it. Reenter the table to find E_f corresponding to this difference, $R_z(E_f)$. In the conversion of $p(E_i)$ to $p(E_f)$, the value of n for polyethylene was taken as 1.81 up to several hundred Mev,* and for steel, $n = 1.77$. The calculation of the

* Actually n decreases slightly with increasing E, and k increases. The error in $p(E)$ caused by neglect of these variations is slight, and results in a few percent overestimate in dose.

final spectrum $p_f(E_f)$ resulting from passage of protons of original spectrum $p_2(E_i)$ through various amounts of steel and polyethylene is a matter of setting up tables to follow this recipe (2) in conjunction with (6). Degraded spectra resulting from such tabulated calculations are plotted in Figure 2, along with the incident spectrum.

The degraded spectra of Figure 2 have been calculated assuming the protons penetrate the shield normally. In actuality non-normal penetration will also take place. Because of this slant penetration, the effective shield thickness will be greater than the actual value, resulting in somewhat lower (perhaps 10 to 30%) fluxes than calculated here.

Nuclear Reactions

As protons pass through the steel shell, or other metal structure on and in a space vehicle, some nuclear interactions will take place. These will be (p, mn), (p, γ) and $(p, p'\gamma)$ events, producing secondaries which are capable of delivering radiation doses to the astronaut. Hence some consideration was given to these effects. Data from various sources were used to estimate cross sections for these processes as a function of energy from a few Mev up to 1000 Mev. Both iron and molybdenum were considered.

The data of Crandall and Millburn [8] were used, along with inelastic scattering cross section data of Hicks and Kirschbaum [9], and others [10, 11, 12], to arrive at the following conclusions regarding neutron production at incident proton energies over 40 Mev: (1) in steel, 0.07 X neutrons per incident proton, and (2) in molybdenum, 0.15 X neutrons per incident proton, where X is the thickness of the vehicle shell in cm, and the protons are distributed in energy according to Equation (1). Consideration of energies below 40 Mev leads to neutron numbers several orders of magnitude less than the higher energy case.

Assuming an approximately constant cross section of 1 barn ($\equiv 10^{-24}$ cm^2) for inelastic collision excitation of nuclei in the vehicle shell, the number of gamma rays generated is 4×10^{-2} X photons/cm^2 (of a few Mev from many nuclear levels) per incident proton/cm^2 where again X is the shell thickness in centimeters.

These neutron and photon energy fluxes are much smaller than those due to direct penetrating protons for most feasible shielding configurations.

Dose Rate Calculations

The proton flux $p(E)$ calculated earlier and plotted in Figure 2 for a given shield represents the differential energy distribution of normally-penetrating protons inside an empty vehicle. This is the flux that would be measured by a radiation detector small enough that self-shielding effects are negligible. The absorbed dose rate in this small detector is related to the differential particle flux $p(E)\ dE$ by

$$\frac{dD}{dt} = 5.76 \times 10^{-5} \int_0^\infty p(E) \frac{dE}{dx}(E)\ dE \text{ rad/hr} \quad (7)$$

where $dE/dx\ (E)$ is the energy loss rate in the detecto in Mev-cm^2/gram, and one rad is 100 ergs/gram.

Equation (7) may be used to calculate the energ absorption rate at any point in a mass of materia provided that $p(E)$ is known at that particular point and dE/dx as a function of energy is known for tha material. Hine and Brownell [13] give data from whic one may obtain $dE/dx\ (E)$ for tissue. This tissue energy absorption rate is plotted as the lower line in Figure 3 On using this curve in Equation (7), along with th appropriate $p(E)$ curve from Figure 2, one obtains a absorbed energy dose rate in a small detector as function of vehicle shielding thickness. These results in tissue rad/hr per unit incident flux, are tabulated i the second column of Table I.

The effectiveness of radiation in causing biologica damage depends not only upon the amount of radian energy absorbed, but also upon the absorbed energy density and upon the biological effect ("end point" being considered. The absorbed energy density i terms of linear energy transfer, kev/micron, will b large for slow-moving heavy particles such as proton of a few Mev. Consequently their effectiveness i enhanced with respect to particles with lower specifi ionization.

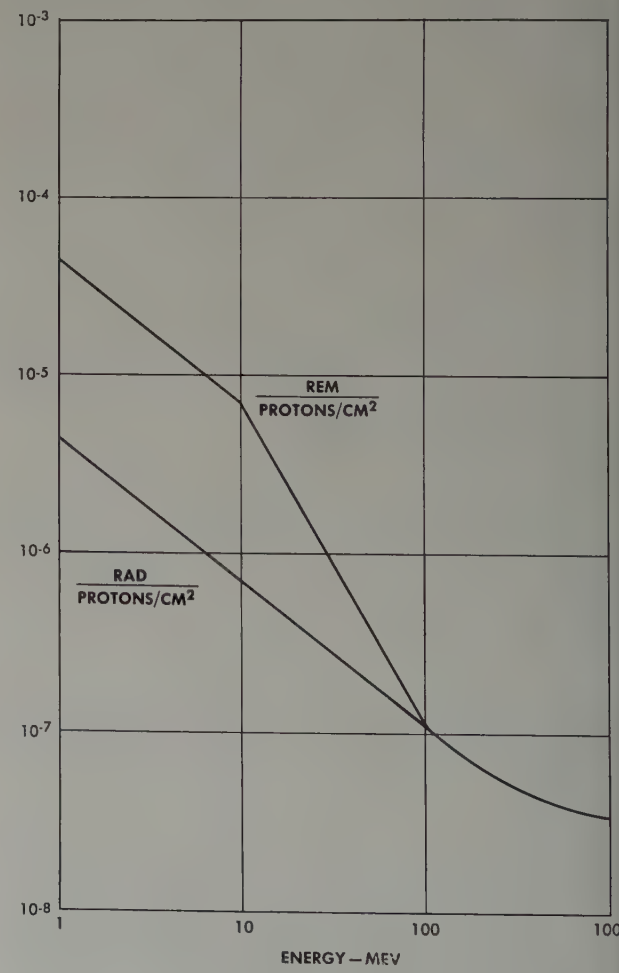


FIG. 3. Lower line—proton absorbed dose in tissue rad pe proton/cm^2 as a function of proton energy. Upper line—as sumed biological dose in rem per proton/cm^2.

TABLE I

Inner Radiation Belt Dose Rates (Protons Only)

Shielding: Steel + CH_2	Small Detector Proton Dose Rates				Body Surface Dose Rate	Body Center Dose Rate
	Unit incident flux		For 2×10^4 p/cm² sec			
(Inches)	*rad/hr* $\times 10^{-8}$	*rem/hr* $\times 10^{-8}$	*rad/hr*	*rem/hr*	*rem/hr*	*rem/hr*
0 + 0	3.5	22	70	440	220	7.0
0 + 1	0.47	3.0	9.3	60	30	6.7
0 + 2	0.29	1.7	5.8	34	17	5.8
0 + 4	0.16	0.83	3.2	16.6	8.3	4.5
0 + 8	0.09	0.38	1.7	7.6	3.8	3.5
0.04 + 0	1.25	8.5	25	170	85	6.6
0.04 + 0.5	0.36	2.3	7.2	45	22.5	6.1
0.04 + 1	0.25	1.5	4.9	30	15	5.7
0.04 + 2	0.19	1.0	3.7	20	10	4.8
0.04 + 4	0.11	0.50	2.1	10.4	5.2	3.6
0.04 + 8	0.06	0.30	1.1	4.8	2.4	2.2
0.10 + 0	0.5	2.5	10	50	25	6.7

Relative Biological Effectiveness (RBE) of a radiation type is defined as the ratio of the absorbed dose of a standard x- or γ-ray quality to the dose of that radiation type required to elicit the same biological effect. A full discussion of the RBE concept and the difficulties with which RBE determinations are fraught is out of place here [14, 15].

In establishing maximum permissible doses for man, and in safety considerations generally, the RBE for heavily ionizing particles is taken to be 10 or 20. For protons up to about 10 Mev, an RBE value of 10 is given by Hine and Brownell, and this value has been taken for the calculations here. In the range 10 Mev to 100 Mev, RBE for protons is here assumed to decrease gradually to 1.0, and from 100 Mev upwards, it is assumed to remain constant at 1.0. The upper curve of Figure 3 shows the assumed rem(E), that is RBE $\times$ rad, per unit incident flux, as a function of the proton energy. In a military situation where safety considerations might give place to strategic ones, an RBE value of 1.0 over the whole energy range might be used, that is, the lower curve of Figure 3. This is equivalent to increasing the allowable dose by a factor of about 5 or 6.

The biological dose rates corresponding to the energy-absorbed dose rates of Table I, Column 2, have been computed by evaluating the expression:

$$\frac{dD}{dt} = 3600 \int_0^\infty p(E)\,\text{rem}\,(E)\,dE \text{ rem/hr}. \quad (8)$$

These dose rates, in rem/hr per unit incident flux, are tabulated in Column 3 of Table I. The ratios of the values in Column 3 to the corresponding values in Column 2, give the effective, or average, RBE value for the particular shielding thickness in question. The effective RBE decreases as shielding thickness increases. This is consistent with the shift of the peak of $p(E)$, Figure 2, to higher energy as thickness increases. Columns 2 and 3 of Table I are applicable to unit incident flux (above 40 Mev), as defined earlier. Columns 4 and 5 give the corresponding total proton dose rates to be expected in the heart of the inner radiation belt, based on present data. Some of these calculated data are also presented in Figures 4 and 5.

The preceding calculations in this section have been for the case of a small detector, in which self-shielding or self-absorption effects are negligible. For an astronaut in a space vehicle, self-shielding of one part of the body by other parts is of considerable importance, in that the dose rate at any given point in the body will be less than the dose rate measured by a small detector at the same location inside the empty shielded vehicle. The exact calculation of the dose rate as a function of depth in tissue would require a detailed knowledge of the orientation of the body and its location inside the vehicle shield, and would involve computing a $p(E)$ distribution at each point in the body. Such a detailed calculation has not been made here. Instead, to make the calculations tractable, we have assumed that the human body can be dosimetrically represented by a sphere of tissue twelve inches in diameter, and that this sphere is located near the center of the shielded volume.

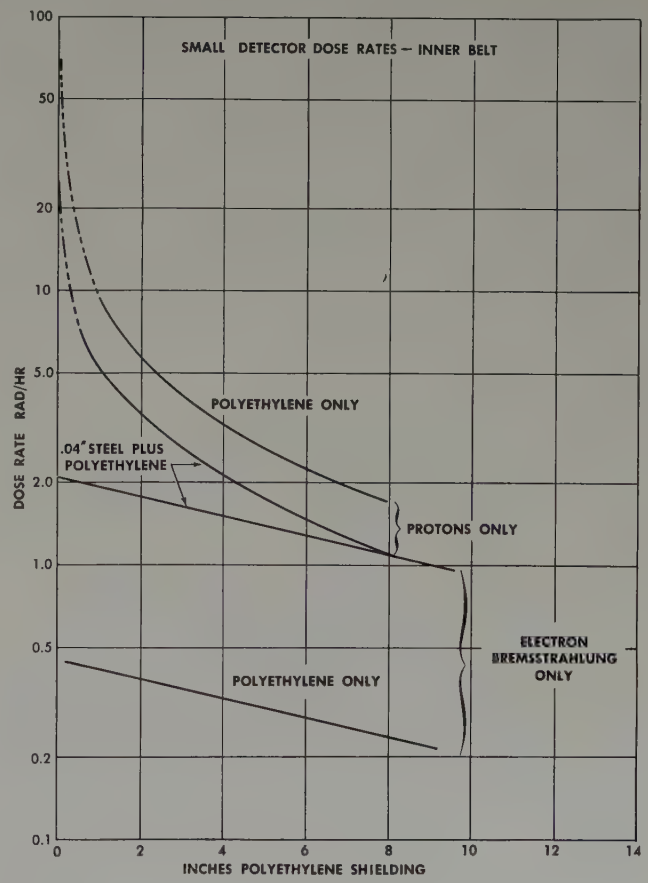


FIG. 4. Absorbed dose rates in rad/hr due to protons and electrons in heart of inner belt, for various polyethylene thicknesses with and without 0.04″ steel vehicle shell. For the region 0 to $\frac{1}{2}$″ for the case of 0.04″ steel and polyethylene, and to 1″ for polyethylene only, the shape of the dose rate curves has been estimated as indicated by the broken lines.

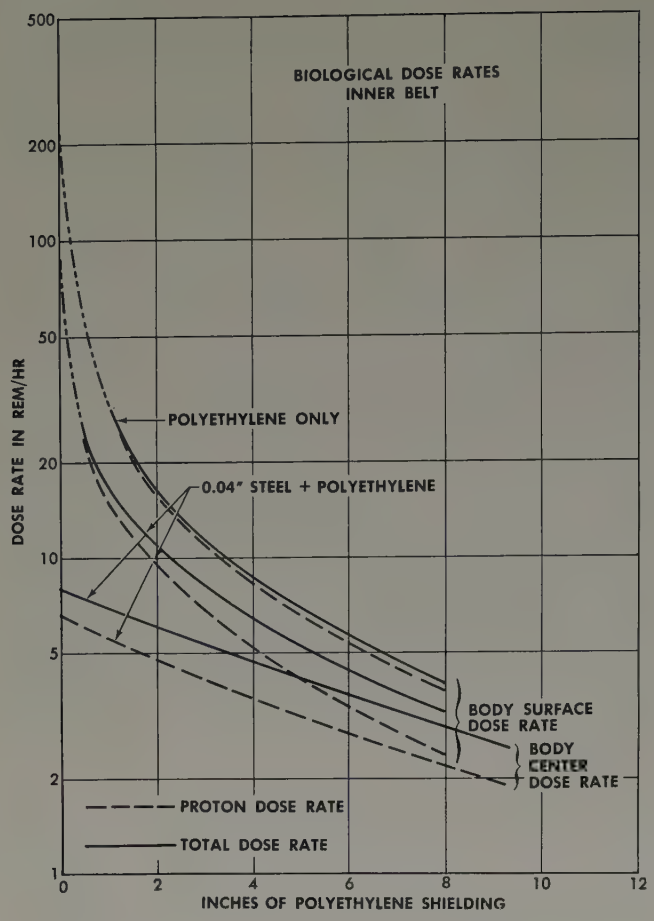


FIG. 5. Biological dose rates, in rem/hr, due to protons and electrons in heart of inner belt, for various polyethylene thicknesses, with and without 0.04″ steel vehicle shell. Dotted lines are dose rates due to protons only. Solid lines are total dose rates due to both electron bremsstrahlung and protons. For the region 0 to ½″ for the case of 0.04″ steel and polyethylene, and to 1″ for polyethylene only, the shape of the body center dose rate curves has been estimated as indicated by the broken lines.

Considering the omnidirectional character of the incident flux, and the proton absorption in the body which gives self-shielding, we estimate that the dose rate on the surface of this tissue sphere is one half the dose rate in a small detector placed at the same point with the sphere removed. These estimated body surface dose rates are tabulated in Column 6 of Table I.

It is possible to calculate the dose rate at the center of this idealized spherical body. In order to use Equation (8), $p(E)$ must be known at the point where the dose rate is desired. This distribution was obtained from those plotted in Figure 2 by further degrading them through six inches of tissue. For each vehicle shielding configuration, the resulting $p(E)$ at the center of the sphere was folded into the rem(E) curve and numerically integrated. The biological dose rates thus calculated are listed in Column 7 of Table I after multiplying by the factor of 2×10^4. These figures are correct for the geometry and other conditions assumed, and reasonably close for the actual situation, the human trunk. These dose rates are also shown in Figure 5.

A more detailed computation has begun, using general incident proton flux parameters, and for various other shielding materials and configurations. As the spectral form of the proton flux becomes better known, more accurate dose calculations will thus be possible.

Electron Doses (Bremsstrahlung)

So far only protons have been considered. In the inner belt, omnidirectional electron flux values of 10^8 cm^{-2} sec^{-1} with energy above 20 kev, and 10^7 cm^{-2} sec^{-1} with energy above 600 kev have been given [2, 4]. These data are consistent with a differential spectrum

$$N_e(E)\,dE = 9.3 \times 10^9 e^{-7.95E}\,dE\,\frac{\text{electrons}}{\text{cm}^2\text{-sec}} \qquad (9)$$

which is used here for want of more definitive spectral information. Less than 1% of the electron energy flux can penetrate a steel shell as thick as 40 mils. For the thick shell case, the bremsstrahlung energy flux produced in the shell by electrons in the energy range E to $E + dE$ is:

$$\Gamma\,dE = \frac{ZE^2}{800} N_e(E)\,dE \qquad (10)$$

or, for steel, and the flux (9),

$$\Gamma\,dE = 3 \times 10^8 E^2 \exp(-7.95E)\,dE\,\frac{\text{Mev}}{\text{cm}^2\text{-sec}}. \qquad (11)$$

The total bremsstrahlung energy is thus:

$$\int_0^\infty \Gamma\,dE = 1.2 \times 10^{-6}\ \text{Mev/cm}^2\text{-sec}. \qquad (12)$$

Dividing by 10^9 incident electrons/cm^2-sec gives a bremsstrahlung energy flux per "unit incident electron flux" of 1.2×10^{-3} Mev/cm^2-sec.

The preceding calculations have made two assumptions concerning bremsstrahlung generation, both of which result in some overestimate of the x-ray doses.

1. The ratio of bremsstrahlung production to ionization loss by electrons, and approximately to total electron energy loss, is given by $EZ/800$. This ratio actually applies to rates of energy loss, but is here used for total energy loss.

2. The direction of the incident electron flux is the direction of the resulting photon flux.

As this photon flux proceeds into the vehicle, it will be attenuated by any further shielding used. The maximum of the distribution function (11) occurs at 0.25 Mev, so a choice of this energy was made as the most probable photon energy. To calculate the reduction in the astronaut's absorbed dose effected by shielding inside the vehicle shell, we have used "poor geometry" attenuation, since scattered photons may also contribute to dose. Alternatively, the total ("good geometry") attenuation coefficients could have been used along with build-up factors. The poor geometry attenuation coefficient for CH_2 at 0.25 Mev is 0.03 cm^2/gram

These considerations lead to dose attenuation factors of 0.93, 0.87, 0.76, 0.58 respectively for 1″, 2″, 4″, and 8″ of polyethylene. Applied to the generated x-ray energy flux of 1.2×10^6 Mev/cm²-sec or 2.4 roentgen/hour, the astronaut's absorbed tissue dose rate is 2.1 rad/hr. The small detector dose rates due to bremsstrahlung are given in Table II, Column 2, and in Figure 4. The body surface dose rate is estimated as three-fourths of the small detector rate, because of self-shielding in the body, and is given in Column 3. The body center dose rates, calculated by considering the attenuation of the x-ray flux in six inches of tissue, are listed in Column 3 of Table II. The contribution of the inner belt electron bremsstrahlung to the astronaut's dose is shown in Figure 5, and is the difference between the solid and dotted curves.

Outer Belt Electrons

Estimates of the outer belt electron fluxes have also been made [2, 4]. These electrons are generally lower energy, there being 10^{11} electrons/cm²-sec, having $E > 0.02$ Mev, and 10^8 electrons/cm²-sec, having $E > 0.2$ Mev. The number of electrons of energy greater than 4 Mev is negligible. The data given are consistent with the differential distribution:

$$N_e(E)\,dE = 8.3 \times 10^{12} e^{-E/.026}\,dE \,\frac{\text{electrons}}{\text{cm}^2\text{-sec}} \quad (13)$$

Using the method outlined in the preceding section, by substituting (13) into (11), the total bremsstrahlung energy generated in a steel shell of thickness greater than a few mils is found to be 9.5×10^6 Mev/cm²-sec. The electron energy for which the maximum bremsstrahlung energy flux occurs is 50 kev, and so this energy was chosen as the most probable photon energy for purposes of calculating absorbed dose and attenuation.

If one assumes that this 50 kev average energy bremsstrahlung flux is generated near the outer surface of the 0.04″ steel shell, then the attenuation and filtering effect of the steel must be considered. Using 1.1 cm²/g as the "poor geometry" attenuation coefficient of steel 0.04″ will reduce the flux by a factor of two. This underestimates the reduction of dose because of the filtering effect of the steel which strongly absorbs the lower energy x-rays by photoelectric processes.

TABLE II

Inner Belt Electron Bremsstrahlung Dose Rates

Shield: Steel + CH_2	Small Detector Dose Rate	Body Surface Dose Rate	Body Center Dose Rate
(*inches*)	*rad/hr for 10^9 elec/cm²-sec*	*rad/hr (= rem/hr)*	*rad/hr (= rem/hr)*
0.04 + 0	2.1	1.6	1.4
0.04 + 1	1.9	1.5	1.3
0.04 + 2	1.8	1.4	1.2
0.04 + 4	1.6	1.2	1.1
0.04 + 8	1.2	0.9	0.7

For no steel (CH_2 only) multiply above figures by 6/26.

At 50 kev, the poor geometry absorption coefficient for CH_2 is 0.03 cm²/gram, and that for tissue was taken as 0.04 cm²/gram. Hence, if no interior shielding is provided, the entire bremsstrahlung flux emerging from the steel shell, namely 4.8×10^6 Mev/cm²-sec will impinge upon the astronaut's body. The resultant "small detector dose rate" is 11.5 tissue rad/hour. The body surface dose rate would be approximately three fourths of this amount. The center dose rate in the idealized spherical body, that is the dose delivered by this flux after passing through six inches of tissue, is 6 rad/hr.

If polyethylene is used for interior shielding, the 50 kev x-ray dose attenuation factors for 1″, 2″, 4″, and 8″ are, respectively, 0.91, 0.82, 0.67 and 0.45. These factors are to be applied to each of the dose rates mentioned, i.e. small detector, body surface, and body center.

The dose rates given here are conservative from the point of view of safety. Lower dose rates would result from the choice of lower atomic number materials for the outer shell. For very thin shells, and no interior shielding, some electrons might penetrate, which could cause skin burn doses. However, in view of the inner belt shielding requirements, it is likely that these direct effects will be eliminated.

Because of current doubts concerning the outer belt electron total flux, it is best to consider these dose rates in terms of a unit incident flux having the spectral form (13). This is obtained by dividing the figures given by 10^{11}. Thus the small detector dose rate is 1.2×10^{-10}, the body surface dose rate is 9×10^{-11}, and the body center dose rate is 6×10^{-11} rad/hr for unit incident flux.

Lack of detailed information regarding the outer belt electron flux energy distribution has justified the types of approximation made here. Refined calculations to eliminate the bremsstrahlung generation and absorption approximations are being made so that, when better flux information becomes available, it may be introduced into these computations to obtain more exact dose rates.

Conclusions

We have calculated the biological dose rates inside a shielded space vehicle due to the protons and electrons which are present in the most intense regions of the radiation belts. The protons in the inner belt are by far the largest contributor to the dose, due to their high energies and relatively great biological effectiveness. The contribution to the dose of secondary radiations due to protons interacting with the shield is small, particularly for thinner shields. The electron-produced contribution is also relatively small, despite the large incident electron flux and the simplified bremsstrahlung-production analysis employed here, which overestimates the bremsstrahlung to be expected.

Another noteworthy point is the rapid decrease of

dose rate, from the unshielded case, with the addition of small amounts of shielding. For thicker shields a given increment of material is less effective in reducing dose rate. This effect can be seen from the curves in Figures 4 and 5. From an engineering and cost standpoint, it would appear better to provide a small amount of shielding and to select vehicle trajectories so that not too much time is spent in the heart of the inner radiation belt.

While the dose rates are lower for the thicker shields, this absorbed energy is distributed more uniformly in the astronaut's body. For the thinner shields, a large fraction of the total dose is absorbed at the body surface. Thus a long-term exposure in the inner radiation belt, which would require a thick shield, will result in near-uniform absorbed dose distribution in the body. A short-term exposure, as might result from rapid passage through the belt, and which would permit thinner shields, would give a larger fraction of the absorbed dose to the body surface. These are additional facts to consider in space trajectory planning.

A more detailed calculation is currently being programmed for automatic computation of biological doses. General parameters specifying radiation belt fluxes and spectra as function of altitude, and general shielding parameters specifying atomic numbers, densities, and thicknesses will be used. Bremsstrahlung calculations will be refined. A body depth-dose calculation will be made. This program should lead to more exact dose rates based on the more reliable particle flux information which is sure to be available in the future.

Acknowledgments

The authors wish to acknowledge the help, in the early phases of this calculation, of Bergene Kawin and Warren Brown, of Boeing Aero-Space Division.

References

[1] Van Allen, J. A. and Frank, L. A., "Radiation Aroun the Earth to a Radial Distance of 107,400 km", Nature **183** (1959), 430

[2] Van Allen, J. A. and Frank, L. A., "Radiation Measure ments to 658,300 km With Pioneer IV," Nature, **18** (1959), 219

[3] Freden, S. C. and White, R. S., "Protons in the Earth' Magnetic Field," Phys. Rev. Letters, **3** (1959), 9

[4] Van Allen, J. A., "Radiation Measurements to 658,30 Kilometers with Pioneer IV," Bulletin A.P.S., Serie II, **4**, No. 7 (1959), p. 402 (Abstract B-10)

[5] Hess, W. N., "Van Allen Belt Protons from Cosmic-Ra Neutron Leakage," Phys. Rev. Letters, **3** (1959), 11

[6] Lenchek, A. M. and Singer, S. F., "Energy Spectrun of Geomagnetically Trapped Protons," Bull. Am. Phys Soc. II, **5** (1959), No. 1, Part I, p. 47 (Abstract N-7)

[7] Rich, M. and Madey, R., "Range-Energy Tables," U of Cal. Report UCRL-2301, March 1954

[8] Crandall, W. E. and Millburn, G. P., "Neutron Pro duction at High Energies," Jour. App. Phys., **29** (1958) 698

[9] Hicks, D. A. and Kirschbaum, A. J., "Total Attenuatio Cross Sections for High-Energy Protons," Livermor Research Laboratory of California Research and De velopment Co., Document MTA-28, December 1952

[10] Glassgold, A. E. and Kellogg, P. J., "Nuclear Scat tering of 40- and 95- Mev Protons," Phys. Rev., **10** (1958), 1291

[11] Hess, W. N., "Summary of High-Energy Nucleon-Nu cleon Cross-Section Data," Rev. Mod. Phys., **30** (1958) 368

[12] Tai, Y. K., Millburn, G. P., Kaplan, S. N., and Moyer B. J., "Neutron Yields from Thick Targets Bombarde by 18- and 32-Mev Protons," Phys. Rev., **109** (1958) 2086

[13] Hine, G. J. and Brownell, G. L., "Radiation Dosi metry," Academic Press (1956), pp. 626, 630

[14] Ibid., pp. 5–7, 11, 289 ff., 661

[15] Report of the International Commission on Radiologica Units and Measurements (ICRU) 1956, N.B.S. Hand book 62.

The Influence of Heart Action and the Circulation of the Blood on Manned Satellite Attitude Control[1]

Lawrence R. Zeitlin[2]

Introduction

Among the internal disturbing forces which must be considered in the design of an attitude control system for a manned satellite are those caused by the physiological processes of the operation, particularly those produced by heart action and the circulation of the blood.

[1] This work was sponsored by the Flight Control Laboratory through a subcontract under Contract AF33(616)-6674 with Systems Corporation of America.

[2] Dunlap and Associates, Inc., Santa Monica, Calif.

1. Ballistic or recoil forces—caused by heartbeat and other impulsive forces.

2. Mass displacement—caused by pooling of blood during sleep, digestion, etc.

3. Torques or couples—caused by dissymmetry o blood flow.

Ballistic or Recoil Forces

It has long been recognized that as a gun kicks when it is fired, so also does the body recoil in response to th

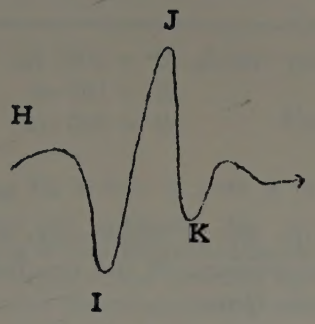


FIG. 1

propelling and impact forces which move the blood in the vascular system.

The recoil motions of the body were first described by Gordon in 1877 and elaborated upon by Henderson in 1905, the honorary godparents of the modern science of ballistocardiography, the study of heart function by the measurement of gross body movement (5).

Essentially, a ballistocardiograph is a spring-suspended bed upon which the subject is tightly strapped. Measuring devices pick off longitudinal motion and amplify it for graphic presentation. When plotted against time, the motions of the ballistocardiograph produce a graph of the general form shown in Fig. 1.

H represents auricular ejections; *I* represents ventricular systole, headward ejection; *J* represents footward motion of blood caused by turn of aorta; and *K* represents the slowing of the downward moving blood.

The equations describing this motion are derived from the principle of conservation of momentum, i.e., mass of ejected blood $\times$ velocity of blood = (mass of body + mass of ballistocardiograph bed) $\times$ velocity (see Fig. 2).

For a standard low frequency ballistocardiograph the movement (D) of the ballistic system in cm. between the I and J peaks can be expressed as:

$$D = \frac{980F}{4\pi^2 f_0^2 (M_1 + M_2)}$$

where f_0 = natural period of the ballistic system
F = force in grams required to move system (1, 7).

If we consider the vehicle and its occupant as an extremely low frequency ballistocardiograph, the recoil forces due to cardiac contractions can be calculated by referring to the equations in the ballistocardiographic literature, substituting the mass of the satellite for that of the ballistocardiograph bed and the restoring force of the attitude control system for that of the ballistocardiograph.

The normal heart pumps approximately 70 ml. of blood from each ventricle, 60 to 80 times per minute. The pressure varies with each portion of the cardiac cycle but the mean pressure in the aorta is about 125 mm Hg. This corresponds to an equivalent rectangular peak of blood velocity of about 113 cm. per second in the aorta, lasting about .2 second per beat. (The

$$M_B \times V_B = (M_1 + M_2) V$$

FIG. 2

actual peak velocity may reach 160 cm./sec. or greater for a much shorter period of time.) (6)

For a 1000 Kg. satellite the displacement due to ventricular contraction would be roughly equal to:

$$d = \frac{V_b \times m_b}{m_s} t$$

$$d = \frac{113 \times 70}{10^6} 2 \times 10^{-1} = 1.58 \times 10^{-3}_{\text{cm}}$$

where V_b = velocity of blood (113 cm/sec)
m_b = mass of blood (70 gm.)
m_s = mass of satellite (1000 Kg.)
t = duration of impulse (approx. 0.2 sec)

This is a trivial displacement except during ultra precise work (i.e., photo mapping, etc.) if the operator is at the center of gravity of the vehicle, but may become more noticeable if the operator is displaced from the center of gravity or if the cardiac rate excites a system resonance.

A check on these calculations is available by recomputing the empirical normal standards for amplitude of displacement for low frequency ballistocardiographs given in the WADC Technical Report 59-593 "Handbook of Circulation" for a combined body and platform weight of 1000 Kg. The actual movement of the subject in space, from the tip of the J wave to the tip of the M wave averages .72 $\times$ 10^{-3} cm. This figure is quite close to that computed from purely speculative information.

Mass Displacement

It is virtually impossible to specify the center of mass or the moment of inertia in three axes of a living animal or man. Factors which may affect center of mass and movement of inertia and hence influence attitude control are, in order of importance:

a. movements of the arms and feet,
b. change of the body position within the restraining unit,
c. changes in the distribution of contents within the digestive tract,
d. blood pooling during various physiological processes.

Because of the variation in the position of the axes, the center of gravity varies accordingly. For man, the position of the center of gravity may, at its best, be described as being located in a sphere with a 10 cm diameter located in the body at roughly the position of the navel. Although there are definite changes in blood distribution, these are minor when compared with the dynamic influence caused by gross movements of the man, shifts of masses caused by digestive processes and changes in mass by metabolism (2), (3), (8).

Torques or Couples

The heart and blood vessels form a closed assemblage of tubes through which the blood is circulated by the action of the heart. The human circulatory system is almost, but not quite, bilaterally symmetrical. There is a slight dissymmetry of blood flow caused by the bend in the aorta which is not compensated for by other blood vessels. Since the bend is to the right, the force tending to rotate the body would be to the left.

The heart and circulation can, for the purpose of estimating system dynamics, be likened to a simple physical circulation model consisting of a pump forcing fluid through a network of tubing. Reduced to its simplest form, this network is a single elliptical loop of tubing with major and minor axes proportionate to the dissymmetry of the circulatory system about the appropriate axes of the body.

Let us assume, for the moment, that the momentum characteristics of the circulatory system can be simulated by considering the entire blood flow taking place in a loop of tubing with a radius of 5 cm. This distance was chosen because cursory measurements of a model of the circulatory system indicated that the RMS distance of major blood vessels and bends in these blood vessels approximated 5 cm. from an arbitrary reference point at the tip of the heart.

The heart of a normal man pumps between 4 and 6 Kg. of blood per minute; or about 7200 Kg. in a 24 hour day. (9) At any time, he has the equivalent of a fluid flywheel within his body with a mass of approximately 5 Kg., a radius of 5 cm., and rotating once a minute.

The angular momentum of a body is defined as the produce of its rotary inertia and the angular velocity around a given axis. For a flywheel with its weight concentrated in the rim, the moment of inertia (I) = MR^2 where M is the mass and R is the radius. Hence the angular momentum of the equivalent blood circuit is:

$$= MR^2W = \frac{(5 \times 10^3)(25)(6.28)}{60} = 1.31 \times 10^4 \text{ gm cm}^2 \text{ radians/second}$$

For a 1000 Kg. satellite, of approximately the shape of the Mercury vehicle, the moment of inertial along its axis is that of a right cone of altitude H radius of base R, and mass M. This is:

$$I = M\tfrac{3}{10} R^2$$

For the Mercury vehicle, $M = 1000$ Kg
$R = 100$ cm
$H = 300$ cm

Hence:

$$I = 10^6 \times 10^4 (.3) = 3 \times 10^9 \text{ gm cm}^2$$

According to the law of conservation of momentun the angular momentums of the two rotating masse must be equal. Hence:

1.31×10^4 gm cm^2 rad./sec. $\quad 3 \times 10^9$ gm cm^2 W
Ang. momentum of blood Ang. momentum of vehicl

$$W = 4.36 \times 10^{-6} \text{ rad./sec.}$$

or

$$2.5 \times 10^4 \text{ deg./sec.}$$

In a 24 hour day, a 1000 Kg. satellite would rotat 21° 40′ about its axis simply in reaction to the angula momentum of the astronaut's circulatory systen Provided the astronaut remained in relatively cor stant orientation to the vehicle, as would be the cas in most small manned satellites, this torque woul affect the attitude of the satellite. Over a long perio of time, a significant amount of energy would be re quired from the attitude control system to counterac this torque.

Notes and References

1. Burger, H. C., Noodergraaf, A. and Verhogen, A. M W., Physical basis of the low frequency ballistocardio graph. *Amer. Heart J.*, **46**, 70–83, 1953.
2. Clamann, H. G., Center of gravity and moments of inerti measurements for a seat plus a Rhesus monkey. *Bioastro nautics*, March 1959, 95–105.
3. Hill, L., The influence of the force of gravity on the cir culation of the blood. *J. Physiol.*, **18**, 15–53, 1895.
4. Lamport, H., Hemodynamics (Chapter 30) *Howell's Text book of Physiology*; Ed. J. F. Fulton, W. B. Saunders Co Philadelphia, 1947.
5. Nickerson, J. L., Ballistocardiography (Chapter) *Medica Physics*, Ed. Otto Glassner, Year Book Publishers, 1950 Chicago, Illinois.
6. Ponder, E., The velocity and pressure of blood flow, (Chap ter 31) *Howell's Textbook of Physiology*; Ed. J. F. Fulton W. B. Saunders Co., Philadelphia, 1947.
7. Rappaport, M. B., Displacement, velocity, and accelera tion ballistocardiograms as registered with an undampe bed of ultralow natural frequency. I. Theory and dynami considerations. *Amer. Heart J.*, **52**, 483–495, 1956.
8. Ward, J. E., Physiological aspects of hypergravic and hypo gravic states. *J. Amer. Med. Assn.*, **172**, 665–668, 1960.
9. WADC Technical Report 59-593, *Handbook of Circulation* Ed. P. L. Altman, October 1959.

Format of Technical Papers for AAS Journal

The editors will appreciate the cooperation of authors in using the following directions for the preparation of manuscripts. These directions have been compiled with a view toward eliminating unnecessary correspondence, avoiding the return of papers for changes, and reducing the charges made for "author's corrections."

Manuscripts

Papers should be submitted in original typewriting (if possible) on one side only of white paper sheets, and should be double or triple spaced with wide margins. However, good quality reproduced copies (e.g. multilith) are acceptable. An additional copy of the paper will facilitate review.

Company Reports

The paper should not be merely a company report. If such a report is to be used as the basis for the paper, appropriate changes should be made in the title page. Lists of figures, tables of contents, and distribution lists should all be deleted.

Titles

The title should be brief, but express adequately the subject of the paper. A footnote reference to the title should indicate any meeting at which the paper has been presented. The name and initials of the author should be written as he prefers; all titles and degrees or honors will be omitted. The name of the organization with which the author is associated should be given in a separate line to follow his name.

Abstracts

An abstract should be provided, preceding the introduction, covering contents of the paper. It should not exceed 200 words.

Headings

The paper can be divided into principal sections as appropriate. Headings or paragraphs are not numbered.

Mathematical Work

As far as possible, formulas should be typewritten. Greek letters and other symbols not available on the typewriter should be carefully inserted in ink. Each such symbol should be identified unambiguously the first time it appears. The distinction between capital and lower-case letters should be clearly shown. Avoid confusion between zero (0) and the letter *O*; between the numeral (1), the letter l, and the prime (′); between alpha and *a*, kappa and *k*, mu and *u*, nu and *v*, eta and *n*.

The level of subscripts, exponents, subscripts to subscripts, and exponents in exponents should be clearly indicated.

Complicated exponents and subscripts should be avoided when possible to represent by a special symbol.

Fractions in the body of the text and fractions occurring in the numerators or denominators of fractions should be written with the solidus. Thus

$$\frac{\cos(\pi x/2b)}{\cos(\pi\alpha/2b)}$$

is the preferred usage.

The intended grouping of handwritten formulas can be made clear by slight variations in spacing, but this procedure is not acceptable in printed formulas. To avoid misunderstanding, the order of symbols should therefore be carefully considered. Thus

$(a + bx)\cos t$ is preferable to $\cos t\,(a + bx)$

In handwritten formulas the size of parentheses, brackets and braces can vary more widely than in print. Particular attention should therefore be paid to the proper use of parentheses, brackets, and braces (which should be used in this order). Thus

$$\{[a + (b + cx)^n]\cos ky\}^2$$

is required rather than $((a + (b + cx)^n)\cos ky)^2$.

Equations are numbered and referred to in text as (15).

Illustrations

Drawings should be made with black India ink on white paper or tracing cloth, and should be at least double the desired size of the cut. Each figure number should be marked with soft pencil in the margin or on the back of the drawing. The width of the lines of such drawings and the size of the lettering must allow for the necessary reduction. Reproducible glossy photographs are acceptable. However, drawings which are unsuitable for reproduction will be returned to the author for redrawing. Legends accompanying the drawings should be typewritten on a separate sheet, properly identified.

Security Clearance

Authors are responsible for the security clearance by an appropriate agency of the material contained in the papers.

Bibliography

References should be grouped together in a bibliography at the end of the manuscript. References to the bibliography should be made by numerals between square brackets [4].

The following examples show the approved arrangements:

for books—[1] HUNSAKER, J. C. and RIGHTMIRE, B. S., *Engineering Applications of Fluid Mechanics*, McGraw-Hill Book Co., New York, 1st ed., 1947, p. 397.

for periodicals—[2] Singer, S. F., "Artificial Modification of the Earth's Radiation Belt," *J. Astronaut. Sci.*, *6* (1959), 1–10.

